

Semi-Implicit finite-difference methods to study the spin-orbit and coherently coupled spinor Bose-Einstein condensates

Paramjeet Banger*, Pardeep Kaur†, Sandeep Gautam‡

June 16, 2021

Abstract

We develop time-splitting finite difference methods, using implicit Backward-Euler and semi-implicit Crank-Nicolson discretization schemes, to study the spin-orbit coupled spinor Bose Einstein condensates with coherent coupling in quasi-one and quasi-two-dimensional traps. The split equations involving kinetic energy and spin-orbit coupling operators are solved using either time implicit Backward-Euler or semi-implicit Crank-Nicolson methods. We explicitly develop the method for pseudospin-1/2, spin-1 and spin-2 condensates. The results for ground states obtained with time-splitting Backward-Euler and Crank-Nicolson methods are in excellent agreement with time-splitting Fourier spectral method which is one of the popular methods to solve the mean-field models for spin-orbit coupled spinor condensates. We confirm the emergence of different phases in spin-orbit coupled pseudospin-1/2, spin-1 and spin-2 condensates with coherent coupling.

1 Introduction

With experimental realization of optical traps [1], all the hyperfine spin states of spin- f ultracold bosonic atoms could be trapped and that led to the discovery of $2f + 1$ component Bose Einstein condensates (BECs) termed as spinor BECs [2]. A spinor condensate can be described by a $2f + 1$ component order parameter that can vary over space and time [3, 4]. Till date, spinor condensates in ultracold gases of spin-1/2 ^{87}Rb [5], spin-1 ^{23}Na [1], spin-1 ^{87}Rb [6], spin-2 ^{23}Na [7], spin-2 ^{87}Rb [6] and spin-3 ^{52}Cr atoms [8] have been experimentally realized. In later experiments [9], spin-orbit coupling (SOC) was also engineered in neutral quantum gases like spinor BECs by controlling the atom light interaction that led to the generation of artificial gauge potentials coupled to the atoms [10, 11, 12]. SOC was first realised experimentally in a BEC of ^{87}Rb [9] by dressing two of its internal spin states from within the ground-state manifold by employing pair of Raman lasers that can create a momentum sensitive coupling between two internal atomic states resulting in an effective Zeeman shift. The

*2018phz0003@iitrpr.ac.in

†2018phz0004@iitrpr.ac.in

‡sandeep@iitrpr.ac.in

strength of SOC can be tuned by Raman laser wavelength, whereas the coherent coupling can be tuned by the laser intensity [13]. SOC and spin-dependent interactions provide a new platform to explore the novel phases in spin-orbit (SO) coupled spinor BECs [14, 15]. In the mean-field approximation, a spin- f BEC in the presence of SO and coherent couplings can be well described by a set of $2f + 1$ coupled nonlinear Gross-Pitaevskii equations (CGPEs) [3, 16, 17, 18]. A wide range of numerical techniques have been employed in literature to study the scalar BEC [19, 20, 21, 22] and spinor BECs [23, 24, 25, 26]. In our earlier works, we also provided sets of Fortran 90/95 codes to solve the mean-field model of SO coupled $f = 1$ [27] and $f = 2$ [28] spinor BECs with Rashba SO-coupling using time-splitting Fourier spectral (TSFS) method. In the present work, we describe time-splitting finite-difference methods to solve the $2f + 1$ CGPEs of spin- f ($f = 1/2, 1, 2$) spinor BECs in quasi-one-dimensional (q1D), quasi-two-dimensional (q2D) traps with SO and coherent couplings. The method can be easily extended to three-dimensional traps and higher spin system (say spin-3 BEC) if needed. We use the time-splitting Backward-Euler (TSBE) or time-splitting Crank-Nicolson (TSCN) finite-difference methods to solve the split equations corresponding to kinetic energy and spin-orbit coupling operators of spin- f BEC. These discretization schemes are employed with periodic boundary conditions and result in $2f + 1$ decoupled sets of linear circulant systems of equations for each spatial dimension. The key property of a circulant matrix is that its columns (rows) can be written in terms of powers of the shift matrix times the first column (row), which allows it to be diagonalized using the discrete Fourier transform [31]. The implementation of TSBE and TSCN is discussed in all its detail for an SO-coupled pseudospin-1/2 condensate, and then extended to higher spin condensates. The rest of this paper is organized as follows: in section 2, we introduce a generic mean-field model suitable to describe the properties SO and coherently coupled pseudospin-1/2, spin-1 and spin-2 BECs. In section 3, we discuss the TSBE and TSCN schemes to numerically solve the CGPEs, i.e. the mean-field model. In section 4, we present the results for energies and component densities corresponding to the stationary states of these spinor BECs having $f = 1/2, 1$ and 2 . We also compare the results of the finite difference methods with the Fourier spectral method.

2 Spinor condensates with spin-orbit and coherent coupling

A generic spin- f condensate with Rashba SO coupling can be modelled at temperatures well below the critical temperature with a matrix equation of form [3, 16]

$$\iota \frac{\partial \Psi}{\partial t} = (H_p + H_{\text{coh}} + H_d + H_{\text{nd}}) \Psi, \quad (1)$$

where Ψ is a $2f + 1$ component order parameter, and $\iota = \sqrt{-1}$. In this work, we consider $f = 1/2, 1, 2$ corresponding, respectively, to pseudospin-1/2, spin-1 and spin-2 condensates. In Eq. (1), H_p and H_{coh} are $2f + 1 \times 2f + 1$ matrix

operators defined as

$$H_p = \mathbf{1} \frac{\hat{p}_x^2 + \hat{p}_y^2 + \hat{p}_z^2}{2} + \gamma(S_x \hat{p}_y - S_y \hat{p}_x), \quad (2)$$

$$H_{\text{coh}} = \frac{\Omega}{2} S_x, \quad (3)$$

where $\mathbf{1}$ represents a $2f+1 \times 2f+1$ identity matrix, γ and Ω are the strengths of SO and coherent couplings, respectively, and $\hat{p}_\nu = -i\partial/\partial\nu$ with $\nu = x, y, z$. S_x and S_y are the irreducible representations of the x and y components of angular momentum operators for spin- f matrix, respectively. The $(m', m)^{\text{th}}$ element of these $2f+1 \times 2f+1$ matrices are

$$(S_x)_{m',m} = \frac{\zeta}{2} \left(\sqrt{(f(f+1) - m'm)} \delta_{m',m+1} + \sqrt{(f(f+1) - m'm)} \delta_{m'+1,m} \right), \quad (4)$$

$$(S_y)_{m',m} = \frac{\zeta}{2i} \left(\sqrt{(f(f+1) - m'm)} \delta_{m',m+1} - \sqrt{(f(f+1) - m'm)} \delta_{m'+1,m} \right), \quad (5)$$

here m' and m vary from $f, f-1, \dots, -f$. In Eqs. (4)-(5) $\zeta = 2$ for $f = 1/2$ and $\zeta = 1$ for $f = 1, 2$. The interatomic interactions in the spinor condensate are accounted by diagonal matrix H_d and non-diagonal matrix H_{nd} . The trapping potential also enters into the H_d matrix. In the present work, we consider the harmonic trapping potential for all the spinor condensates. These matrices for a pseudospin-1/2 condensate are [16]

$$H_d = \begin{pmatrix} V + \sum_{l=1}^2 g_{1l} |\psi_l|^2 & 0 \\ 0 & V + \sum_{l=1}^2 g_{2l} |\psi_l|^2 \end{pmatrix}, \quad H_{\text{nd}} = 0, \quad (6)$$

where

$$V = \frac{1}{2} \sum_{\nu} \alpha_{\nu}^2 \nu^2, \quad g_{ll} = \frac{4\pi N a_{ll}}{a_{\text{osc}}}, \quad g_{l,3-l} = \frac{4\pi N a_{l,3-l}}{a_{\text{osc}}},$$

where g_{ll} and $g_{l,3-l}$ with $l = 1, 2$ are intra- and inter-species interaction strengths, respectively, a_{osc} is the oscillator length chosen as a unit of length, N is the total number of particles in the condensate, $\alpha_{\nu} = \omega_{\nu}/\omega_x$ with $\nu = x, y, z$ is the ratio of confining-potential frequencies along ν th direction to x direction. The intraspecies interaction strengths are defined in terms of s -wave scattering lengths, a_{11} and a_{22} , whereas interspecies interaction strength is defined in terms of interspecies s -wave scattering length $a_{12} = a_{21}$. Similarly, these matrices for spin-1 condensate are [3, 17, 29]

$$H_d = \begin{pmatrix} V + c_0 \rho + c_1 (\rho_0 + \rho_-) & 0 & 0 \\ 0 & V + c_0 \rho + c_1 \rho_+ & 0 \\ 0 & 0 & V + c_0 \rho + c_1 (\rho_0 - \rho_-) \end{pmatrix}, \quad (7a)$$

$$H_{\text{nd}} = c_1 \begin{pmatrix} 0 & \psi_0 \psi_{-1}^* & 0 \\ \psi_0^* \psi_{-1} & 0 & \psi_0^* \psi_1 \\ 0 & \psi_0 \psi_1^* & 0 \end{pmatrix}, \quad (7b)$$

here $\rho_l = |\psi_l|^2$ with $l = 0, \pm 1$, $\rho = \sum_l \rho_l$, and $\rho_{\pm} = \rho_{+1} \pm \rho_{-1}$ and

$$c_0 = \frac{4\pi N (a_0 + 2a_2)}{3a_{\text{osc}}}, \quad c_1 = \frac{4\pi N (a_2 - a_0)}{3a_{\text{osc}}}. \quad (8)$$

The interaction strengths c_0 and c_1 are defined in terms of s -wave scattering lengths a_0 and a_2 . The subscript 0 or 2 in the scattering length characterises the total spin of the allowed scattering channel. Lastly, H_d and H_{nd} for a spin-2 condensate are [3, 18]

$$H_d = \text{diag}(h_{+2}, h_{+1}, h_0, h_{-1}, h_{-2}), \quad (9a)$$

$$H_{nd} = \begin{pmatrix} 0 & h_{12} & h_{13} & 0 & 0 \\ h_{12}^* & 0 & h_{23} & 0 & 0 \\ h_{13}^* & h_{23}^* & 0 & h_{34} & h_{35} \\ 0 & 0 & h_{34}^* & 0 & h_{45} \\ 0 & 0 & h_{35}^* & h_{45}^* & 0 \end{pmatrix}, \quad (9b)$$

where

$$\begin{aligned} h_{\pm 2} &= V + c_0 \rho \pm 2c_1 F_z + \frac{2}{5} c_2 |\psi_{\mp 2}|^2, & h_0 &= V + c_0 \rho + \frac{1}{5} c_2 |\psi_0|^2, \\ h_{\pm 1} &= V + c_0 \rho \pm c_1 F_z + \frac{2}{5} c_2 |\psi_{\mp 1}|^2, & h_{12} &= c_1 F_- - \frac{2}{5} c_2 \psi_{-1} \psi_{-2}^*, \\ h_{13} &= \frac{1}{5} c_2 \psi_0 \psi_{-2}^*, & h_{23} &= \frac{\sqrt{6}}{2} c_1 F_- - \frac{1}{5} c_2 \psi_0 \psi_{-1}^*, \\ h_{34} &= \frac{\sqrt{6}}{2} c_1 F_- - \frac{1}{5} c_2 \psi_1 \psi_0^*, & h_{35} &= \frac{1}{5} c_2 \psi_2 \psi_0^*, & h_{45} &= c_1 F_- - \frac{2}{5} c_2 \psi_2 \psi_1^*, \end{aligned}$$

and

$$F_z = \sum_{l=-2}^2 l |\psi_l|^2, \quad F_- = F_+^* = 2\psi_{-2}^* \psi_{-1} + \sqrt{6} \psi_{-1}^* \psi_0 + \sqrt{6} \psi_0^* \psi_1 + 2\psi_2 \psi_1^*, \quad (10a)$$

$$c_0 = \frac{4\pi N(4a_2 + 3a_4)}{7a_{\text{osc}}}, \quad c_1 = \frac{4\pi N(a_4 - a_2)}{7a_{\text{osc}}}, \quad c_2 = \frac{4\pi N(7a_0 - 10a_2 + 3a_4)}{7a_{\text{osc}}}. \quad (10b)$$

In Eq. (10b), c_0, c_1 , and c_2 are three interaction parameters, and a_0, a_2, a_4 are the s -wave scattering lengths in the permitted scattering channels.

The order parameter for three spin systems is normalized to unity as

$$\int \sum_l |\psi_l(\mathbf{x}, t)|^2 d\mathbf{x} = \sum_l \mathcal{N}_l = 1. \quad (11)$$

The order parameter's norm along with the energy of these SO coupled spinor condensate, which is defined as

$$E = \int \left[\sum_{l,m} \psi_l^* (H_p + H_{\text{coh}} + H_d + H_{nd})_{lm} \psi_m \right] d\mathbf{x}, \quad (12)$$

where l, m run over species' labels, are the two conserved quantities for an SO-coupled condensate. In the present work, the species' labels are 1, 2 for pseudospin-1/2, 1, 0, -1 for spin-1 and 2, 1, 0, -1, -2 for spin-2 BECs. The species' labels 1 and 2 for pseudospin-1/2 BEC are equivalents of labels 1/2 and -1/2, respectively, used in this work. For the sake of the compactness of the notations, the explicit functional dependence of V on \mathbf{x} and ψ_l on \mathbf{x} and t has been suppressed.

3 Time-splitting Finite difference methods

We describe the (semi)-implicit finite-difference schemes to numerically solve the coupled Gross–Pitaevskii equations (CGPEs) for SO-coupled spinor condensates. We use time-splitting Backward-Euler (TSBE) and time-splitting Crank-Nicolson (TSCN) methods to solve the coupled sets of non-linear partial differential equations describing SO-coupled pseudospin-1/2, spin-1 and spin-2 BECs. The implementation is explained in all its detail for an SO-coupled pseudospin-1/2 condensate, and then extended to higher spin condensates. The results obtained with these finite difference schemes are compared with results from Fourier spectral method. The latter method has been used by us to solve CGPEs for SO-coupled spin-1 [27] and spin-2 condensates [28].

3.1 SO-coupled Pseudospin-1/2 Condensate

3.1.1 Quasi-one-dimensional pseudospin-1/2 BEC

We consider a two-component pseudospin-1/2 BEC confined by a harmonic trapping potential with Rashba SO and coherent couplings. We first elaborate the method for solving one-dimensional CGPEs which describe an SO-coupled pseudospin-1/2 BEC trapped by a q1D trapping potential. In such a trap, the y and z coordinates can be integrated out and after a rotation by $\pi/2$ about z -axis in spin-space which changes S_y to $-S_x$, the resultant matrix operator H_p is

$$H_p = \mathbf{1} \frac{\hat{p}_x^2}{2} - \gamma S_y \hat{p}_x \equiv \mathbf{1} \frac{\hat{p}_x^2}{2} + \gamma S_x \hat{p}_x, \quad (13)$$

where $\mathbf{1}$ is a 2×2 identity matrix, and S_x and S_y are Pauli spin matrices. The form of H_{coh} , H_d , and H_{nd} remain same as in Eqs. (3) and (6) with the caveat that

$$\mathbf{x} = x, \quad V = \frac{1}{2} \alpha_x^2 x^2, \quad g_{ll} = \frac{2N a_{ll} \sqrt{\alpha_y \alpha_z}}{a_{osc}}, \quad g_{l,3-l} = \frac{2N a_{l,3-l} \sqrt{\alpha_y \alpha_z}}{a_{osc}},$$

where the terms have the same meanings as described in the previous section. The time evolution of an SO-coupled spinor condensate as per Eq. (1) is approximated by a first order operator splitting, wherein one is required to solve the following equations successively over the same period

$$\iota \frac{\partial \Psi}{\partial t} = H_p \Psi, \quad (14a)$$

$$\iota \frac{\partial \Psi}{\partial t} = H_{\text{coh}} \Psi, \quad (14b)$$

$$\iota \frac{\partial \Psi}{\partial t} = H_d \Psi, \quad (14c)$$

where $\Psi(\mathbf{x}, t) = [\psi_1(\mathbf{x}, t), \psi_2(\mathbf{x}, t)]^T$ with T denoting the transpose. The matrix Eq. (14a) in terms of coupled component equations is

$$\iota \frac{\partial \psi_l(x, t)}{\partial t} = -\frac{1}{2} \frac{\partial^2 \psi_l(x, t)}{\partial x^2} - \iota \gamma \frac{\partial \psi_{3-l}(x, t)}{\partial x}, \quad (15a)$$

where $l = 1, 2$ is species' label. The spatial domain $x \in [-L_x/2, L_x/2)$ is discretized via N_x uniformly spaced points with a spacing of Δx . The resulting

one-dimensional space grid is $x_i = -L_x/2 + (i-1)\Delta x$ where $i = 1, 2, \dots, N_x$. Using Δt as the time-step to discretize time, the discrete analogue of $\psi_l(x, t)$ is $\phi_{(i,l)}^n$ which represents the value of l th component of the order parameter at spatial coordinate x_i at time $n\Delta t$. The discretization scheme employs the periodic boundary conditions by ensuring that

$$\phi_{(1,l)}^n = \phi_{(N_x+1,l)}^n, \quad \phi_{(0,l)}^n = \phi_{(N_x,l)}^n. \quad (16)$$

In the present work, indices l and m are exclusively used for species' labels, indices i and j are used to denote only space-grid point, n is the index used for time, and $\nu = x, y, z$. The discrete analogue of Eq. (15a) using Backward-Euler or Crank-Nicolson discretization schemes is

$$\begin{aligned} \phi_{(i,l)}^{n+1} - \phi_{(i,l)}^n &= \frac{\iota\Delta t}{4\Delta x^2} \left[\alpha \left(\phi_{(i+1,l)}^{n+1} - 2\phi_{(i,l)}^{n+1} + \phi_{(i-1,l)}^{n+1} \right) + \beta \left(\phi_{(i+1,l)}^n - 2\phi_{(i,l)}^n \right. \right. \\ &\quad \left. \left. + \phi_{(i-1,l)}^n \right) \right] - \frac{\gamma\Delta t}{4\Delta x} \left[\alpha \left(\phi_{(i+1,3-l)}^{n+1} - \phi_{(i-1,3-l)}^{n+1} \right) + \beta \left(\phi_{(i+1,3-l)}^n \right. \right. \\ &\quad \left. \left. - \phi_{(i-1,3-l)}^n \right) \right], \end{aligned} \quad (17)$$

where $\alpha = 2, \beta = 0$ for Backward-Euler discretization, and $\alpha = \beta = 1$ for Crank-Nicolson discretization. The local truncation error incurred in Backward-Euler and Crank-Nicolson discretizations are, respectively, of the order $O(\Delta x^2 + \Delta t)$ and $O(\Delta x^2 + \Delta t^2)$ [30]. Considering *Backward-Euler* discretization first, Eq. (17) is

$$\iota \frac{\phi_{(i,l)}^{n+1} - \phi_{(i,l)}^n}{\Delta t} = - \frac{\phi_{(i+1,l)}^{n+1} - 2\phi_{(i,l)}^{n+1} + \phi_{(i-1,l)}^{n+1}}{2\Delta x^2} - \iota\gamma \frac{\phi_{(i+1,3-l)}^{n+1} - \phi_{(i-1,3-l)}^{n+1}}{2\Delta x}.$$

For $l = 1, 2$, the time evolution as per Backward-Euler is equivalent to

$$\begin{bmatrix} \phi_{(i,1)}^{n+1} \\ \phi_{(i,2)}^{n+1} \end{bmatrix} = (\mathbf{1} + \iota H_p \Delta t)^{-1} \begin{bmatrix} \phi_{(i,1)}^n \\ \phi_{(i,2)}^n \end{bmatrix}, \quad (18)$$

where

$$H_p \begin{bmatrix} \phi_{(i,1)}^{n+1} \\ \phi_{(i,2)}^{n+1} \end{bmatrix} = \begin{bmatrix} -\frac{\phi_{(i+1,1)}^{n+1} - 2\phi_{(i,1)}^{n+1} + \phi_{(i-1,1)}^{n+1}}{2\Delta x^2} - \iota\gamma x \frac{\phi_{(i+1,2)}^{n+1} - \phi_{(i-1,2)}^{n+1}}{2\Delta x} \\ -\frac{\phi_{(i+1,2)}^{n+1} - 2\phi_{(i,2)}^{n+1} + \phi_{(i-1,2)}^{n+1}}{2\Delta x^2} - \iota\gamma x \frac{\phi_{(i+1,1)}^{n+1} - \phi_{(i-1,1)}^{n+1}}{2\Delta x} \end{bmatrix}. \quad (19)$$

As H_p is an Hermitian operator, time evolution operator $(\mathbf{1} + \iota H_p \Delta t)^{-1}$ in Backward-Euler discretization is not unitary leading to the norm being not conserved. In contrast to this, the time evolution as per Crank-Nicolson is equivalent to

$$\begin{bmatrix} \phi_{(i,1)}^{n+1} \\ \phi_{(i,2)}^{n+1} \end{bmatrix} = \frac{\mathbf{1} - \iota H_p \Delta t}{\mathbf{1} + \iota H_p \Delta t} \begin{bmatrix} \phi_{(i,1)}^n \\ \phi_{(i,2)}^n \end{bmatrix}, \quad (20)$$

corresponding to a unitary operator $(\mathbf{1} - \iota H_p \Delta t)/(\mathbf{1} + \iota H_p \Delta t)$. The Backward-Euler method is therefore not suitable for realtime evolution in contrast to Crank-Nicolson method. Nonetheless, in imaginary time evolution, a non-unitary time evolution, used to obtain the stationary state solutions both Backward-

Euler or Crank-Nicolson methods can be used. Rewriting Eq. (17) as

$$\begin{aligned} & -\frac{\iota\alpha\Delta t}{4\Delta x^2} \left[\phi_{(i-1,l)}^{n+1} + \phi_{(i+1,l)}^{n+1} \right] + \left(1 + \frac{\iota\alpha\Delta t}{2\Delta x^2} \right) \phi_{(i,l)}^{n+1} + \frac{\gamma\alpha\Delta t}{4\Delta x} \left(\phi_{(i+1,3-l)}^{n+1} - \phi_{(i-1,3-l)}^{n+1} \right) \\ & = \frac{\iota\beta\Delta t}{4\Delta x^2} \left[\phi_{(i-1,l)}^n + \phi_{(i+1,l)}^n \right] + \left(1 - \frac{\iota\beta\Delta t}{2\Delta x^2} \right) \phi_{(i,l)}^n - \frac{\gamma\beta\Delta t}{4\Delta x} \left(\phi_{(i+1,3-l)}^n - \phi_{(i-1,3-l)}^n \right). \end{aligned} \quad (21)$$

Using Eq. (16) in Eq. (21) with $i = 1, 2, \dots, N_x$ and $l = 1, 2$, the resulting set of $2N_x$ coupled linear algebraic equations can be written in matrix form as

$$A\Phi_l^{n+1} + B\Phi_{3-l}^{n+1} = D_l, \quad (22)$$

where A, B are circulant $N_x \times N_x$ matrices and Φ_l^{n+1} , D_l are $N_x \times 1$ matrices. These matrices can be expressed as

$$A(i, :) = \left(1 + \frac{\iota\alpha\Delta t}{2\Delta x^2}, -\frac{\iota\alpha\Delta t}{4\Delta x^2}, 0, \dots, 0, -\frac{\iota\alpha\Delta t}{4\Delta x^2} \right) (C^{i-1})^T, \quad (23a)$$

$$B(i, :) = \left(0, \frac{\alpha\Delta t\gamma}{4\Delta x}, 0, \dots, 0, -\frac{\alpha\Delta t\gamma}{4\Delta x} \right) (C^{i-1})^T, \quad (23b)$$

$$\Phi_l^{n+1} = \left(\phi_{(1,l)}^{n+1}, \phi_{(2,l)}^{n+1}, \phi_{(3,l)}^{n+1}, \dots, \phi_{(N_x,l)}^{n+1} \right)^T, \quad (23c)$$

$$\begin{aligned} d_l(i) = & \left[\frac{\iota\beta\Delta t}{4\Delta x^2} \left\{ \phi_{(i-1,l)}^n + \phi_{(i+1,l)}^n \right\} + \left(1 - \frac{\iota\beta\Delta t}{2\Delta x^2} \right) \phi_{(i,l)}^n \right. \\ & \left. - \frac{\gamma\beta\Delta t}{4\Delta x} \left(\phi_{(i+1,3-l)}^n - \phi_{(i-1,3-l)}^n \right) \right], \end{aligned} \quad (23d)$$

where $A(i, :)$ and $B(i, :)$ are the i th rows of A and B, respectively, $d_l(i)$ is the i th element of column matrix D_l , and C is defined as

$$C = \begin{bmatrix} 0 & 0 & \dots & 1 \\ 1 & 0 & \dots & 0 \\ \vdots & \ddots & & \vdots \\ 0 & \dots & 1 & 0 \end{bmatrix}. \quad (24)$$

For $l = 1, 2$, Eq. (22) represents two coupled matrix equations which can be decoupled to yield

$$(B^2 - A^2)\Phi_l^{n+1} = BD_{3-l} - AD_l, \quad (25)$$

which for $l = 1$ and 2 represents two decoupled sets of linear circulant system of equations. Now, $B^2 - A^2$ being a circulant matrix, it can be diagonalised using Fourier matrix as [31]

$$B^2 - A^2 = F^{-1}\Lambda F, \quad \text{where} \quad (26a)$$

$$F_{i,j} = \frac{1}{\sqrt{N_x}} \exp \left[-\frac{2\pi\iota l}{N_x} (i-1)(j-1) \right], \quad \text{and} \quad (26b)$$

$$\Lambda = \text{diag}[\sqrt{N_x} F \{ B^2(:, 1) - A^2(:, 1) \}]. \quad (26c)$$

Now, the product of the Fourier matrix (F) with a one-dimensional array is equal to the discrete Fourier transform of the array, and hence the solution to Eq. (25) using Eqs. (26a)-(26c) is [31]

$$\Phi_l^{n+1} = \text{IDFT} \left(\text{DFT}(BD_{3-l} - AD_l) ./ \text{DFT}(B^2(:, 1) - A^2(:, 1)) \right), \quad (27)$$

where DFFT and IDFT stand for discrete forward Fourier and inverse discrete Fourier transforms, respectively, $A^2(:, 1)$ and $B^2(:, 1)$ denote the first columns of A^2 and B^2 , and $./$ indicates the element wise division. Now, Eq. (14b) is evolved in time from $t_n = n\Delta t$ to $t_{n+1} = (n+1)\Delta t$ considering Eq. (27) as the solution at t_n . The exact analytic solution to Eq. (14b) is

$$\Psi(\mathbf{x}, t_{n+1}) = \exp[-\iota H_{\text{coh}}\Delta t] \Psi(\mathbf{x}, t_n) = \left[\mathbf{1} \cos\left(\frac{\Omega\Delta t}{2}\right) - \iota S_x \sin\left(\frac{\Omega\Delta t}{2}\right) \right] \Psi(\mathbf{x}, t_n). \quad (28)$$

The last step involves solving Eq. (14c) over the same period treating the solution in Eq. (28) as the solution at $t_n = n\Delta t$. The exact solution to Eq. (14c) is

$$\Psi(\mathbf{x}, t_{n+1}) = \exp[-\iota H_{\text{d}}\Delta t] \Psi(\mathbf{x}, t_n). \quad (29)$$

Quasi-two-dimensional pseudospin-1/2 BEC

In a quasi-two-dimensional trap with tight confinement along z axis, the form of matrix operator H_{p} after integrating out the z coordinate becomes

$$H_{\text{p}} = \mathbf{1} \frac{\hat{p}_x^2 + \hat{p}_y^2}{2} + \gamma(S_x \hat{p}_y - S_y \hat{p}_x), \quad (30)$$

whereas the form H_{coh} , H_{d} , H_{nd} again remain unchanged from those in Eqs. (3) and (6) with a caveat that

$$\mathbf{x} \equiv (x, y), \quad V = \frac{1}{2}(\alpha_x^2 x^2 + \alpha_y^2 y^2), \quad g_{lm} = \frac{2N a_{lm} \sqrt{2\pi\alpha_z}}{a_{osc}}. \quad (31)$$

Using the time-splitting, the time evolution of the condensate from t_n to t_{n+1} is approximated by successive solutions to the following equations over the same period

$$\iota \frac{\partial \Psi}{\partial t} = H_{p_x} \Psi, \quad (32a)$$

$$\iota \frac{\partial \Psi}{\partial t} = H_{p_y} \Psi, \quad (32b)$$

$$\iota \frac{\partial \Psi}{\partial t} = H_{\text{coh}} \Psi, \quad (32c)$$

$$\iota \frac{\partial \Psi}{\partial t} = H_{\text{d}} \Psi, \quad (32d)$$

where H_{p_x} and H_{p_y} are defined as

$$H_{p_x} = \mathbf{1} \frac{\hat{p}_x^2}{2} - \gamma S_y \hat{p}_x, \quad H_{p_y} = \mathbf{1} \frac{\hat{p}_y^2}{2} + \gamma S_x \hat{p}_y. \quad (33)$$

Here, we consider a two-dimensional spatial grid defined as $\nu_i = -L_\nu/2 + (i-1)\Delta\nu$, where $i = 1, 2, \dots, N_\nu$, $\nu = x, y$, and $\Delta\nu$ is spatial step size. The discrete

analogue of component wavefunction is $\phi_{(i,j,l)}^n$ which is equal to value of the l th wavefunction at space point (x_i, y_j) at t_n time. Similar to quasi-one-dimensional condensates, finite difference equivalents of each of Eq. (32a) and Eq. (32b) can be simplified to two decoupled matrix equations

$$(B_x^2 + A_x^2)X_l^{n+1} = A_x D_l^x + (-1)^l B_x D_{3-l}^x, \quad (34a)$$

$$(B_y^2 - A_y^2)Y_l^{n+1} = B_y D_{3-l}^y - A_y D_l^y, \quad (34b)$$

where A_ν, B_ν (with $\nu = x, y$), $X_l^{n+1}, Y_l^{n+1}, D_l^\nu$ are defined

$$A_\nu(i, :) = \left(1 + \frac{\iota\alpha\Delta t}{2\Delta\nu^2}, -\frac{\iota\alpha\Delta t}{4\Delta\nu^2}, 0, \dots, 0, -\frac{\iota\alpha\Delta t}{4\Delta\nu^2} \right) (C^{i-1})^T, \quad (35a)$$

$$B_x(i, :) = \left(0, \frac{\iota\alpha\Delta t\gamma}{4\Delta x}, 0, \dots, 0, -\frac{\iota\alpha\Delta t\gamma}{4\Delta x} \right) (C^{i-1})^T, \quad (35b)$$

$$B_y(i, :) = \left(0, \frac{\alpha\Delta t\gamma}{4\Delta y}, 0, \dots, 0, -\frac{\alpha\Delta t\gamma}{4\Delta y} \right) (C^{i-1})^T, \quad (35c)$$

$$X_l^{n+1} = \left(\phi_{(1,j,l)}^{n+1}, \phi_{(2,j,l)}^{n+1}, \phi_{(3,j,l)}^{n+1}, \dots, \phi_{(N_x,j,l)}^{n+1} \right)^T, \quad (35d)$$

$$Y_l^{n+1} = \left(\phi_{(i,1,l)}^{n+1}, \phi_{(i,2,l)}^{n+1}, \phi_{(i,3,l)}^{n+1}, \dots, \phi_{(i,N_y,l)}^{n+1} \right)^T, \quad (35e)$$

$$d_l^x(i) = \left[\frac{\iota\beta\Delta t}{4\Delta x^2} \left\{ \phi_{(i-1,j,l)}^n + \phi_{(i+1,j,l)}^n \right\} + \left(1 - \frac{\iota\beta\Delta t}{2\Delta x^2} \right) \phi_{(i,j,l)}^n + \frac{(-1)^l \iota\gamma\beta\Delta t}{4\Delta x} \left(\phi_{(i+1,j,3-l)}^n - \phi_{(i-1,j,3-l)}^n \right) \right], \quad (35f)$$

$$d_l^y(i) = \left[\frac{\iota\beta\Delta t}{4\Delta y^2} \left\{ \phi_{(i,j-1,l)}^n + \phi_{(i,j+1,l)}^n \right\} + \left(1 - \frac{\iota\beta\Delta t}{2\Delta y^2} \right) \phi_{(i,j,l)}^n - \frac{\gamma\beta\Delta t}{4\Delta y} \left(\phi_{(i,j+1,3-l)}^n - \phi_{(i,j-1,3-l)}^n \right) \right], \quad (35g)$$

where $A_\nu(i, :)$ and $B_\nu(i, :)$ are the i th row of A_ν and B_ν , respectively, $d_l^\nu(i)$ is the i th element of column matrix D_l^ν , and C is defined in Eq. (24). For a fixed value of j (y -index) and l (species index), Eqs. (34a) is a linear circulant system of equations which can be solved by the same procedure as discussed to solve Eq. (25). The solution to Eq. (32a) is obtained by solving Eq. (34a) for all j and l values following exactly the same procedure as discussed Sec. 3.1.1. This solution, then, is considered as an input solution at t_n while solving another set of linear circulant system of Eqs. (34b) over the same period from t_n to $t_n + \Delta t$. The solutions to Eqs. (32c)-(32d) are again given as in Eqs. (28)-(29) with $\Psi(\mathbf{x}, t_n) = [\psi_1(x, y, t_n), \psi_2(x, y, t_n)]^T$ with T standing for transpose.

3.2 SO-coupled spin-1 condensate

3.2.1 Quasi-one-dimensional spin-1 BEC

In quasi-one-dimensional trap, H_p for an SO-coupled spin-1 BEC takes the form

$$H_p = \mathbf{1} \frac{\hat{p}_x^2}{2} + \gamma S_x \hat{p}_x, \quad (36)$$

where $\mathbf{1}$ is a 3×3 identity matrix, and S_x is the 3×3 spin-1 matrix. The form of H_{coh} , H_{d} , and H_{nd} in Eqs. (3), (7a), (7b) remain unchanged, provided

$$\mathbf{x} = x, \quad V = \frac{1}{2}\alpha_x^2 x^2, \quad c_0 = \sqrt{\alpha_y \alpha_z} \frac{2N(a_0 + 2a_2)}{3a_{\text{osc}}}, \quad c_1 = \sqrt{\alpha_y \alpha_z} \frac{2N(a_2 - a_0)}{3a_{\text{osc}}}.$$

Using the first order time-splitting, the solution of the Eq. (1) is equivalent to solving following equations successively

$$\iota \frac{\partial \Psi}{\partial t} = H_{\text{p}} \Psi, \quad (37a)$$

$$\iota \frac{\partial \Psi}{\partial t} = (H_{\text{nd}} + H_{\text{coh}}) \Psi = H_{\text{nd}+} \Psi, \quad (37b)$$

$$\iota \frac{\partial \Psi}{\partial t} = H_{\text{d}} \Psi. \quad (37c)$$

where $H_{\text{nd}+} = H_{\text{nd}} + H_{\text{coh}}$, and $\Psi(\mathbf{x}, t) = [\psi_1(\mathbf{x}, t), \psi_0(\mathbf{x}, t), \psi_{-1}(\mathbf{x}, t)]^T$. We solve Eq. (37a) using finite difference schemes described in detail for pseudospin-1/2 BEC. Using Backward-Euler (and/or Crank-Nicolson) discretization schemes along with periodic boundary conditions, viz. Eq. (16), Eq. (37a) reduces to three coupled matrix equations

$$A\Phi_{\pm 1}^{n+1} + B\Phi_0^{n+1} = D_{\pm 1}, \quad (38a)$$

$$A\Phi_0^{n+1} + B(\Phi_1^{n+1} + \Phi_{-1}^{n+1}) = D_0. \quad (38b)$$

Eqs. (38a)-(38b), can be decoupled into following three independent matrix equations,

$$(2B^2A - A^3)\Phi_{\pm 1}^{n+1} = (B^2 - A^2)D_{\pm 1} + ABD_0 - B^2D_{\mp 1}, \quad (39a)$$

$$(A^2 - 2B^2)\Phi_0^{n+1} = AD_0 - B(D_1 + D_{-1}), \quad (39b)$$

where A and Φ_l^{n+1} with $l = 1, 0, -1$ are same as in Eq. (23a) and Eq. (23c), respectively, whereas rows of B and elements of D_j are now defined as

$$B(i, :) = \left(0, \frac{\alpha \Delta t \gamma}{4\sqrt{2}\Delta x}, 0, \dots, 0, -\frac{\alpha \Delta t \gamma}{4\sqrt{2}\Delta x} \right) (C^{i-1})^T \quad (40a)$$

$$d_{\pm 1}(i) = \left[\frac{\iota \beta \Delta t}{4\Delta x^2} \left\{ \phi_{(i-1, \pm 1)}^n + \phi_{(i+1, \pm 1)}^n \right\} + \left(1 - \frac{\iota \beta \Delta t}{2\Delta x^2} \right) \phi_{(i, \pm 1)}^n - \frac{\gamma \beta \Delta t}{4\sqrt{2}\Delta x} \left(\phi_{(i+1, 0)}^n - \phi_{(i-1, 0)}^n \right) \right] \quad (40b)$$

$$d_0(i) = \left[\frac{\iota \beta \Delta t}{4\Delta x^2} \left\{ \phi_{(i-1, 0)}^n + \phi_{(i+1, 0)}^n \right\} + \left(1 - \frac{\iota \beta \Delta t}{2\Delta x^2} \right) \phi_{(i, 0)}^n - \frac{\gamma \beta \Delta t}{4\sqrt{2}\Delta x} \left(\phi_{(i+1, 1)}^n - \phi_{(i-1, 1)}^n + \phi_{(i+1, -1)}^n - \phi_{(i-1, -1)}^n \right) \right]. \quad (40c)$$

The decoupled matrix Eqs. (39a) -(39b) are linear circulant system of equations which can be solved by using the method described for pseudospin-1/2 BEC. The analytic solution to Eq. (37b) is [27]

$$\Psi(\mathbf{x}, t_{n+1}) \approx \left(\mathbf{1} + \frac{\cos \zeta - 1}{\zeta^2} \Delta t^2 H_{\text{nd}+}^2 - \iota \frac{\sin \zeta}{\zeta} \Delta t H_{\text{nd}+} \right) \Psi(\mathbf{x}, t_n), \quad (41)$$

where $\zeta = \Delta t \sqrt{|c_1 \psi_0 \psi_{-1}^* + \frac{\Omega}{2\sqrt{2}}|^2 + |c_1 \psi_0 \psi_1^* + \frac{\Omega}{2\sqrt{2}}|^2}$. Finally, the solution to Eq. (37c) is again given as in Eq. (29) with the caveat that the various quantities are identified as those corresponding to spin-1 BEC.

Quasi-two-dimensional spin-1 BEC

Here the form of matrix operator H_p is same as in Eq. (30) with $\mathbf{1}$ representing a 3×3 identity matrix, and S_ν with $\nu = x, y$ denoting the spin-1 matrices. Also, the form of H_{coh} , H_d , and H_{nd} in Eqs. (3), (7a), (7b), respectively, remain unchanged, provided

$$\mathbf{x} \equiv (x, y), \quad V = \sum_{\nu=x,y} \frac{\alpha_\nu^2 \nu^2}{2}, \quad (42)$$

$$c_0 = \sqrt{2\pi\alpha_z} \frac{2N(a_0 + 2a_2)}{3a_{\text{osc}}}, \quad c_1 = \sqrt{2\pi\alpha_z} \frac{2N(a_2 - a_0)}{3a_{\text{osc}}}. \quad (43)$$

The CGPEs of a quasi-2D spin-1 BEC with Rashba SO coupling can be split into following set of equations, and these has to be solved successively over the same period.

$$\iota \frac{\partial \Psi}{\partial t} = H_{p_x} \Psi, \quad (44a)$$

$$\iota \frac{\partial \Psi}{\partial t} = H_{p_y} \Psi, \quad (44b)$$

$$\iota \frac{\partial \Psi}{\partial t} = (H_{\text{nd}} + H_{\text{coh}}) \Psi = H_{\text{nd}+} \Psi, \quad (44c)$$

$$\iota \frac{\partial \Psi}{\partial t} = H_d \Psi. \quad (44d)$$

where H_{p_x} and H_{p_y} are defined in Eq. (33) with $\mathbf{1}$, and S_ν being identified as 3×3 identity and spin-1 matrices, respectively. Similar to quasi-two-dimensional pseudospin-1/2 BEC, each of Eq. (44a) and Eq. (44b) can be discretized into three decoupled matrix equations, such as

$$(A_x^3 + 2A_x B_x^2) X_{\pm 1}^{n+1} = (A_x^2 + B_x^2) D_{\pm 1}^x \mp A_x B_x D_0^x + B_x^2 D_{\mp 1}^x, \quad (45a)$$

$$(A_x^2 + 2B_x^2) X_0^{n+1} = A_x D_0^x + B_x (D_1^x - D_{-1}^x) \quad (45b)$$

for Eq. (44a), and

$$(2B_y^2 A_y - A_y^3) Y_{\pm 1}^{n+1} = (B_y^2 - A_y^2) D_{\pm 1}^y + A_y B_y D_0^y - B_y^2 D_{\mp 1}^y, \quad (46a)$$

$$(A_y^2 - 2B_y^2) Y_0^{n+1} = A_y D_0^y - B_y (D_1^y + D_{-1}^y), \quad (46b)$$

for Eq. (44b). Here, A_ν (with $\nu = x, y$), X_l^{n+1} , Y_l^{n+1} , are defined as in Eq. (35a), Eq. (35d) and Eq. (35e) respectively, whereas B_ν, D_l^ν are now defined as

$$B_x(i, :) = \left(0, \frac{\iota\alpha\Delta t\gamma}{4\sqrt{2}\Delta x}, 0, \dots, 0, -\frac{\iota\alpha\Delta t\gamma}{4\sqrt{2}\Delta x} \right) (C^{i-1})^T \quad (47a)$$

$$B_y(i, :) = \left(0, \frac{\alpha\Delta t\gamma}{4\sqrt{2}\Delta y}, 0, \dots, 0, -\frac{\alpha\Delta t\gamma}{4\sqrt{2}\Delta y} \right) (C^{i-1})^T \quad (47b)$$

$$d_{\pm 1}^x(i) = \left[\frac{\iota\beta\Delta t}{4\Delta x^2} \left\{ \phi_{(i-1,j,\pm 1)}^n + \phi_{(i+1,j,\pm 1)}^n \right\} + \left(1 - \frac{\iota\beta\Delta t}{2\Delta x^2} \right) \phi_{(i,j,\pm 1)}^n \right. \\ \left. \mp \frac{\iota\gamma\beta\Delta t}{4\sqrt{2}\Delta x} \left(\phi_{(i+1,j,0)}^n - \phi_{(i-1,j,0)}^n \right) \right] \quad (47c)$$

$$d_0^x(i) = \left[\frac{\iota\beta\Delta t}{4\Delta x^2} \left\{ \phi_{(i-1,j,0)}^n + \phi_{(i+1,j,0)}^n \right\} + \left(1 - \frac{\iota\beta\Delta t}{2\Delta x^2} \right) \phi_{(i,j,0)}^n \right. \\ \left. + \frac{\iota\beta\Delta t\gamma}{4\sqrt{2}\Delta x} \left(\phi_{(i+1,j,1)}^n - \phi_{(i-1,j,1)}^n - (\phi_{(i-1,j,-1)}^n - \phi_{(i+1,j,-1)}^n) \right) \right]. \quad (47d)$$

$$d_{\pm 1}^y(i) = \left[\frac{\iota\beta\Delta t}{4\Delta y^2} \left\{ \phi_{(i,j-1,\pm 1)}^n + \phi_{(i,j+1,\pm 1)}^n \right\} + \left(1 - \frac{\iota\beta\Delta t}{2\Delta y^2} \right) \phi_{(i,j,\pm 1)}^n \right. \\ \left. - \frac{\gamma\beta\Delta t}{4\sqrt{2}\Delta y} \left(\phi_{(i,j+1,0)}^n - \phi_{(i,j-1,0)}^n \right) \right] \quad (47e)$$

$$d_0^y(i) = \left[\frac{\iota\beta\Delta t}{4\Delta y^2} \left\{ \phi_{(i,j-1,0)}^n + \phi_{(i,j+1,0)}^n \right\} + \left(1 - \frac{\iota\beta\Delta t}{2\Delta y^2} \right) \phi_{(i,j,0)}^n \right. \\ \left. - \frac{\gamma\beta\Delta t}{4\sqrt{2}\Delta y} \left(\phi_{(i,j+1,1)}^n - \phi_{(i,j-1,1)}^n + \phi_{(i,j+1,-1)}^n - \phi_{(i,j-1,-1)}^n \right) \right]. \quad (47f)$$

Eqs. (45a)-(45b) and (46a)-(46b) are linear circulant system of equations, and thus can be solved as described for pseudospin-1/2 condensates in Sec. 3.1.1. The solution to Eqs. (44c)-(44d) is similar as described for quasi-one-dimensional spin-1 condensates.

3.3 SO-coupled spin-2 condensate

3.3.1 Quasi-one-dimensional spin-2 BEC

Similar to quasi-one-dimensional pseudospin-1/2 and spin-1 BECs, form of H_p is $\mathbf{1}\hat{p}_x^2/2 + \gamma S_x \hat{p}_x$ where S_x denotes the spin-2 matrix and forms of H_{coh} , H_d and H_{nd} remain the same as in Eqs. (3), (9a), and (9b), respectively. The trapping potential and interaction parameters are

$$V(\mathbf{x}) = \frac{\alpha_x^2 x^2}{2}, \quad c_0 = \sqrt{\alpha_y \alpha_z} \frac{2N(4a_2 + 3a_4)}{7a_{\text{osc}}}, \quad (48a)$$

$$c_1 = \sqrt{\alpha_y \alpha_z} \frac{2N(a_4 - a_2)}{7a_{\text{osc}}}, \quad c_2 = \sqrt{\alpha_y \alpha_z} \frac{2N(7a_0 - 10a_2 + 3a_4)}{7a_{\text{osc}}} \quad (48b)$$

Using the first order time-splitting, the solution of the Eq. (1) is equivalent to solving following equations successively

$$\iota \frac{\partial \Psi}{\partial t} = H_p \Psi, \quad (49a)$$

$$\iota \frac{\partial \Psi}{\partial t} = (H_{\text{nd}} + H_{\text{coh}}) \Psi = H_{\text{nd}+} \Psi, \quad (49b)$$

$$\iota \frac{\partial \Psi}{\partial t} = H_d \Psi, \quad (49c)$$

where $H_{\text{nd}+} = H_{\text{nd}} + H_{\text{coh}}$, and $\Psi(\mathbf{x}, t) = [\psi_2(\mathbf{x}, t), \psi_1(\mathbf{x}, t), \psi_0(\mathbf{x}, t), \psi_{-1}(\mathbf{x}, t), \psi_{-2}(\mathbf{x}, t)]^T$. Similar to pseudospin-1/2 and spin-1 condensates, finite difference discretization of Eq. (49a) along with periodic boundary conditions, viz. Eq. (16), reduces it to five decoupled matrix equations

$$\begin{aligned} A(A^2 - B^2)(A^3 - 4AB^2)\Phi_{\pm 2}^{n+1} = & -\sqrt{\frac{3}{2}}(B^4 - A^2B^2)D_0 - \frac{3}{2}AB^3D_{\mp 1} \\ & + \frac{3}{2}B^4D_{\mp 2} + \left(\frac{5}{2}AB^3 - BA^3\right)D_{\pm 1} \\ & + \left(\frac{3}{2}B^4 + A^4 - 4A^2B^2\right)D_{\pm 2}, \end{aligned} \quad (50a)$$

$$\begin{aligned} (A^2 - B^2)(A^3 - 4AB^2)\Phi_{\pm 1}^{n+1} = & \sqrt{\frac{3}{2}}(B^3 - A^2B)D_0 - \frac{3}{2}B^3D_{\mp 2} + \\ & \frac{3}{2}AB^2D_{\mp 1} + \left(A^3 - \frac{5}{2}AB^2\right)D_{\pm 1} \\ & + \left(\frac{5}{2}B^3 - A^2B\right)D_{\pm 2}, \end{aligned} \quad (50b)$$

$$\begin{aligned} (A^3 - 4AB^2)\Phi_0^{n+1} = & (A^2 - B^2)D_0 - \sqrt{\frac{3}{2}}AB(D_1 + D_{-1}) \\ & + \sqrt{\frac{3}{2}}B^2(D_2 + D_{-2}), \end{aligned} \quad (50c)$$

where A , B , and Φ_l^{n+1} are same as in Eq. (23a), (23b) and (23c) respectively, whereas the elements of column matrices D_l with $l = 2, 1, 0, -1, -2$ are

$$\begin{aligned} d_{\pm 2}(i) = & \left[\frac{\iota\beta\Delta t}{4\Delta x^2} \left\{ \phi_{(i-1, \pm 2)}^n + \phi_{(i+1, \pm 2)}^n \right\} + \left(1 - \frac{\iota\beta\Delta t}{2\Delta x^2}\right) \phi_{(i, \pm 2)}^n \right. \\ & \left. - \frac{\gamma\beta\Delta t}{4\Delta x} \left(\phi_{(i+1, \pm 1)}^n - \phi_{(i-1, \pm 1)}^n \right) \right], \end{aligned} \quad (51a)$$

$$\begin{aligned} d_{\pm 1}(i) = & \left[\frac{\iota\beta\Delta t}{4\Delta x^2} \left\{ \phi_{(i-1, \pm 1)}^n + \phi_{(i+1, \pm 1)}^n \right\} + \left(1 - \frac{\iota\beta\Delta t}{2\Delta x^2}\right) \phi_{(i, \pm 1)}^n - \frac{\gamma\beta\Delta t}{4\Delta x} \right. \\ & \left. \times \left(\phi_{(i+1, \pm 2)}^n - \phi_{(i-1, \pm 2)}^n \right) - \sqrt{\frac{3}{2}} \frac{\gamma\beta\Delta t}{4\Delta x} \left(\phi_{(i+1, 0)}^n - \phi_{(i-1, 0)}^n \right) \right], \end{aligned} \quad (51b)$$

$$\begin{aligned} d_0(i) = & \left[\frac{\iota\beta\Delta t}{4\Delta x^2} \left\{ \phi_{(i-1, 0)}^n + \phi_{(i+1, 1)}^n \right\} + \left(1 - \frac{\iota\beta\Delta t}{2\Delta x^2}\right) \phi_{(i, 0)}^n - \sqrt{\frac{3}{2}} \frac{\gamma\beta\Delta t}{4\Delta x} \right. \\ & \left. \times \left(\phi_{(i+1, 1)}^n - \phi_{(i-1, 1)}^n \right) - \sqrt{\frac{3}{2}} \frac{\gamma\beta\Delta t}{4\Delta x} \left(\phi_{(i+1, -1)}^n - \phi_{(i-1, -1)}^n \right) \right]. \end{aligned} \quad (51c)$$

The five decoupled sets of linear circulant system of Eqs. (50a)-(50c) can be solved as discussed in Sec. 3.1.1. The detailed procedure to solve Eq. (49b) is discussed in the appendix, and the exact solution to Eq. (49c) is same as in Eq. (29).

3.4 Quasi-two-dimensional spin-2 BEC

Here the form of matrix operator H_{p_ν} is same as in Eq. (30) with $\mathbf{1}$ representing a 5×5 identity matrix, S_ν are spin-2 matrices and the forms of H_{coh} , H_{d} , and H_{nd} in Eqs. (3), (9a), (9b), respectively, remain unchanged, with

$$\mathbf{x} \equiv (x, y), \quad V = \sum_{\nu=x,y} \frac{\alpha_\nu^2 \nu^2}{2}, \quad c_0 = \sqrt{2\pi\alpha_z} \frac{2N(4a_2 + 3a_4)}{7a_{\text{osc}}}, \quad (52)$$

$$c_1 = \sqrt{2\pi\alpha_z} \frac{2N(a_4 - a_2)}{7a_{\text{osc}}}, \quad c_2 = \sqrt{2\pi\alpha_z} \frac{2N(7a_0 - 10a_2 + 3a_4)}{7a_{\text{osc}}}. \quad (53)$$

Here also, similar to quasi-two-dimensional spin-1 BEC, each of Eq. (44a) and (44b) can be discretized into five decoupled matrix equations, such as

$$\begin{aligned} (4A_x B_x^2 + A_x^3)(B_x^2 + A_x^2)A_x X_{\pm 2}^{n+1} &= \sqrt{\frac{3}{2}}(B_x^4 + A_x^2 B_x^2)D_0^x \mp \frac{3}{2}A_x B_x^3 D_{\mp 1}^x \\ &+ \frac{3}{2}B_x^4 D_{\mp 2}^x \mp \left(\frac{5}{2}A_x B_x^3 + B_x A_x^3\right)D_{\pm 1}^x \\ &+ \left(\frac{3}{2}B_x^4 + A_x^4 + 4A_x^2 B_x^2\right)D_{\pm 2}^x, \end{aligned} \quad (54a)$$

$$\begin{aligned} (4A_x B_x^2 + A_x^3)(B_x^2 + A_x^2)X_{\pm 1}^{n+1} &= \mp \sqrt{\frac{3}{2}}(B_x^3 + A_x^2 B_x)D_0^x \mp \frac{3}{2}B_x^3 D_{\mp 2}^x \\ &\pm \left(\frac{5}{2}B_x^3 + A_x^2 B_x\right)D_{\pm 2}^x + \frac{3}{2}A_x B_x^2 D_{\mp 1}^x \\ &+ \left(\frac{5}{2}A_x B_x^2 + A_x^3\right)D_{\pm 1}^x, \end{aligned} \quad (54b)$$

$$\begin{aligned} (4A_x B_x^2 + A_x^3)X_0^{n+1} &= (B_x^2 + A_x^2)D_0^x + \sqrt{\frac{3}{2}}A_x B_x (D_1^x - D_{-1}^x) \\ &+ \sqrt{\frac{3}{2}}B_x^2 (D_2^x + D_{-2}^x) \end{aligned} \quad (54c)$$

for Eq. (44a), and

$$\begin{aligned}
A_y(A_y^2 - B_y^2)(A_y^3 - 4A_yB_y^2)Y_{\pm 2}^{n+1} &= -\sqrt{\frac{3}{2}}(B_y^4 - A_y^2B_y^2)D_0^y - \frac{3}{2}A_yB_y^3D_{\mp 1}^y \\
&+ \frac{3}{2}B_y^4D_{\mp 2}^y + \left(\frac{5}{2}A_yB_y^3 - B_yA_y^3\right)D_{\pm 1}^y \\
&+ \left(\frac{3}{2}B_y^4 + A_y^4 - 4A_y^2B_y^2\right)D_{\pm 2}^y, \tag{55a}
\end{aligned}$$

$$\begin{aligned}
(A_y^2 - B_y^2)(A_y^3 - 4A_yB_y^2)Y_{\pm 1}^{n+1} &= \sqrt{\frac{3}{2}}(B_y^3 - A_y^2B_y)D_0^y + \frac{3}{2}A_yB_y^2D_{\mp 1}^y \\
&- \frac{3}{2}B_y^3D_{\mp 2}^y + \left(A_y^3 - \frac{5}{2}A_yB_y^2\right)D_{\pm 1}^y \\
&+ \left(\frac{5}{2}B_y^3 - A_y^2B_y\right)D_{\pm 2}^y, \tag{55b}
\end{aligned}$$

$$\begin{aligned}
(A_y^3 - 4A_yB_y^2)Y_0^{n+1} &= (A_y^2 - B_y^2)D_0^y - \sqrt{\frac{3}{2}}A_yB_y(D_1^y + D_{-1}^y) \\
&+ \sqrt{\frac{3}{2}}B_y^2(D_2^y + D_{-2}^y) \tag{55c}
\end{aligned}$$

for Eq. (44b). A_ν (with $\nu = x, y$), X_l^{n+1} , and Y_l^{n+1} are defined as in Eq. (35a), Eq. (35d) and Eq. (35e) respectively, and B_ν, D_l^ν are now defined as

$$B_x(i, :) = \left(0, \frac{\iota\alpha\Delta t\gamma}{4\Delta x}, 0, \dots, 0, -\frac{\iota\alpha\Delta t\gamma}{4\Delta x}\right) (C^{i-1})^T, \tag{56a}$$

$$B_y(i, :) = \left(0, \frac{\alpha\Delta t\gamma}{4\Delta y}, 0, \dots, 0, -\frac{\alpha\Delta t\gamma}{4\Delta y}\right) (C^{i-1})^T, \tag{56b}$$

$$\begin{aligned}
d_{\pm 2}^x(i) &= \left[\frac{\iota\beta\Delta t}{4\Delta x^2} \left\{\phi_{(i-1,j,\pm 2)}^n + \phi_{(i+1,j,\pm 2)}^n\right\} + \left(1 - \frac{\iota\beta\Delta t}{2\Delta x^2}\right) \phi_{(i,j,\pm 2)}^n\right. \\
&\quad \left.\mp \frac{\iota\gamma\beta\Delta t}{4\Delta x} \left(\phi_{(i+1,j,\pm 1)}^n - \phi_{(i-1,j,\pm 1)}^n\right)\right], \tag{56c}
\end{aligned}$$

$$\begin{aligned}
d_{\pm 1}^x(i) &= \left[\frac{\iota\beta\Delta t}{4\Delta x^2} \left\{\phi_{(i-1,j,\pm 1)}^n + \phi_{(i+1,j,\pm 1)}^n\right\} + \left(1 - \frac{\iota\beta\Delta t}{2\Delta x^2}\right) \phi_{(i,j,\pm 1)}^n\right. \\
&\quad \left.\pm \frac{\iota\gamma\beta\Delta t}{4\Delta x} \left(\phi_{(i+1,j,\pm 2)}^n - \phi_{(i-1,j,\pm 2)}^n\right) \mp \sqrt{\frac{3}{2}} \frac{\iota\gamma\beta\Delta t}{4\Delta x} \left(\phi_{(i+1,j,0)}^n - \phi_{(i-1,j,0)}^n\right)\right], \tag{56d}
\end{aligned}$$

$$\begin{aligned}
d_0^x(i) &= \left[\frac{\iota\beta\Delta t}{4\Delta x^2} \left\{\phi_{(i-1,j,0)}^n + \phi_{(i+1,j,1)}^n\right\} + \left(1 - \frac{\iota\beta\Delta t}{2\Delta x^2}\right) \phi_{(i,j,0)}^n\right. \\
&\quad \left.+ \sqrt{\frac{3}{2}} \frac{\iota\gamma\beta\Delta t}{4\Delta x} \left(\phi_{(i+1,j,1)}^n - \phi_{(i-1,j,1)}^n\right) - \sqrt{\frac{3}{2}} \frac{\iota\gamma\beta\Delta t}{4\Delta x} \left(\phi_{(i+1,j,-1)}^n - \phi_{(i-1,j,-1)}^n\right)\right], \tag{56e}
\end{aligned}$$

$$d_{\pm 2}^y(i) = \left[\frac{\iota\beta\Delta t}{4\Delta y^2} \left\{ \phi_{(i,j-1,\pm 2)}^n + \phi_{(i,j+1,\pm 2)}^n \right\} + \left(1 - \frac{\iota\beta\Delta t}{2\Delta y^2} \right) \phi_{(i,\pm 2)}^n - \frac{\gamma\beta\Delta t}{4\Delta y} \left(\phi_{(i,j+1,\pm 1)}^n - \phi_{(i,j-1,\pm 1)}^n \right) \right], \quad (57a)$$

$$d_{\pm 1}^y(i) = \left[\frac{\iota\beta\Delta t}{4\Delta y^2} \left\{ \phi_{(i,j-1,\pm 1)}^n + \phi_{(i,j+1,\pm 1)}^n \right\} + \left(1 - \frac{\iota\beta\Delta t}{2\Delta y^2} \right) \phi_{(i,j,\pm 1)}^n - \frac{\gamma\beta\Delta t}{4\Delta y} \times \left(\phi_{(i,j+1,\pm 2)}^n - \phi_{(i,j-1,\pm 2)}^n \right) - \sqrt{\frac{3}{2}} \frac{\gamma\beta\Delta t}{4\Delta y} \left(\phi_{(i,j+1,0)}^n - \phi_{(i,j-1,0)}^n \right) \right], \quad (57b)$$

$$d_0^y(i) = \left[\frac{\iota\beta\Delta t}{4\Delta y^2} \left\{ \phi_{(i,j-1,0)}^n + \phi_{(i,j+1,1)}^n \right\} + \left(1 - \frac{\iota\beta\Delta t}{2\Delta y^2} \right) \phi_{(i,j,0)}^n - \sqrt{\frac{3}{2}} \frac{\gamma\beta\Delta t}{4\Delta y} \times \left(\phi_{(i,j+1,1)}^n - \phi_{(i,j-1,1)}^n \right) - \sqrt{\frac{3}{2}} \frac{\gamma\beta\Delta t}{4\Delta y} \left(\phi_{(i,j+1,-1)}^n - \phi_{(i,j-1,-1)}^n \right) \right]. \quad (57c)$$

where $B_\nu(i, :)$ is the i th row of B_ν and $d_l^y(i)$ is the i th element of column matrix D_l^y . Eqs. (54a)-(54c) and (55a)-(55c) are linear circulant system of equations, and thus can be solved in a similar manner as described for pseudospin-1/2 and spin-1 condensates. The solution to Eqs. (44c)-(44d) is on similar lines as described for quasi-one-dimensional spin-2 condensates.

4 Numerical Results

Here, we present the numerical results with TSBE and TSCN methods for the pseudospin-1/2, spin-1, and spin-2 in the presence as well as absence of coherent coupling. Both TSBE and TSCN can be used to obtain the ground state solutions of an SO and coherently coupled spinor BEC. This can be achieved by considering an initial guess solution to the CGPEs and replacing t by $-it = \tilde{t}$ to solve CGPEs. The resultant imaginary time evolution is not norm preserving, and hence total norm needs to be fixed to unity after each time iteration. The quantity $\tau = \max |\phi_{(i,j,l)}^{n+1} - \phi_{(i,j,l)}^n| / \Delta\tilde{t}$ serves as the convergence criterion to quantify convergence in imaginary time propagation. The stationary state solutions reported in this section have been obtained with $\tau = 10^{-6}$. In contrast to imaginary time evolution, realtime dynamics of the spinor BECs can be studied with TSCN and not with TSBE as the later does not conserve norm as was discussed in Sec. 3.1.1.

4.1 Pseudospin-1/2

For pseudospin-1/2 case, we choose an experimentally realizable ^{87}Rb pseudospinor-1/2 BEC with scattering length $a_{11} = 101.8a_B$, interaction strengths $g_{12} = 1.1g_{11}$, $g_{22} = 0.9g_{11}$ and $g_{12} = g_{21}$, where a_B is the Bohr radius. We consider 5000 atoms trapped in q1D trapping potential with $\omega_x = 2\pi \times 20\text{Hz}$,

$\omega_y = 2\pi \times 400\text{Hz}$ and $\omega_z = 2\pi \times 400\text{Hz}$. The interaction strengths in dimensionless units are given as

$$(g_{11}, g_{22}, g_{12}) = (446.95, 402.26, 491.65), \quad (58)$$

with $g_{12} = g_{21}$. For q2D BEC, we consider 5000 atoms of ^{87}Rb in a trap with trapping frequencies $\omega_x = \omega_y = 2\pi \times 20\text{Hz}$, $\omega_z = 2\pi \times 400\text{Hz}$. For this case, the interaction strengths $g_{22} = 0.9g_{11}$, $g_{12} = 1.1g_{11}$, and $g_{12} = g_{21}$ for $a_{11} = 101.8a_B$ are given as

$$(g_{11}, g_{22}, g_{12}) = (250, 225, 275), \quad (59)$$

with $g_{12} = g_{21}$. In both these cases, we compare the results from TSFS, TSBE and TSCN in the presence as well as absence of coherent coupling and find an excellent agreement. The comparison of the ground state energies obtained with three methods for different values of γ are given in Table-1 for $\Omega = 0$ and Table-2 for $\Omega = 0.5$. The results with TSBE and TSCN are in very good agreement with those from TSFS.

Table 1: Comparison of ground state energies of pseudospin-1/2 BEC of ^{87}Rb obtained with TSFS, TSBE and TSCN for different values of γ in the absence of coherent coupling Ω . The interaction strength parameters are $g_{11} = 446.95$, $g_{22} = 402.26$ and $g_{12} = g_{21} = 491.65$ for q1D BEC, whereas the same for q2D BEC are $g_{11} = 250.52$, $g_{22} = 225.47$ and $g_{12} = g_{21} = 275.57$.

		$\Delta x = 0.1, \Delta \tilde{t} = 0.01$			$\Delta x = 0.1, \Delta \tilde{t} = 0.005$		
		TSFS	TSBE	TSCN	TSFS	TSBE	TSCN
q1D	$\gamma = 0.5$	21.4357	21.4357	21.4357	21.4357	21.4357	21.4357
	$\gamma = 1.0$	21.4186	21.4186	21.4186	21.4186	21.4186	21.4186
	$\gamma = 1.5$	21.3333	21.3334	21.3333	21.3324	21.3324	21.3324
	$\gamma = 2.0$	20.7018	20.7035	20.7022	20.7001	20.7014	20.7011
q2D	$\gamma = 0.5$	5.7201	5.7201	5.7201	5.7201	5.7201	5.7201
	$\gamma = 1.0$	5.4707	5.4707	5.4707	5.4707	5.4707	5.4707
	$\gamma = 1.5$	4.8520	4.8520	4.8520	4.8518	4.8518	4.8518
	$\gamma = 2.0$	3.9783	3.9786	3.9787	3.9883	3.9786	3.9786

The component densities corresponding to ground state solutions obtained with TSBE and TSCN methods for q1D ^{87}Rb BEC are shown in Fig. 1. The densities obtained with two methods are in an excellent agreement. Similarly, the component densities, obtained with TSCN method, for q2D ^{87}Rb BEC for different values of γ and Ω are shown in Fig. 2. We also study the variation of the convergence criterion as a function of \tilde{t} in imaginary-time propagation with TSBE, TSCN, and TSFS to obtain the ground state solution. As an example, in the imaginary-time propagation to obtain the ground state of q1D pseudospin-1/2 BEC of ^{87}Rb starting with normalized Gaussian initial guess wavefunctions for the two components, the variation of τ as a function of \tilde{t} , obtained with three methods, is shown in Fig. 3(a) for $\Delta x = 0.1$ and $\Delta \tilde{t} = 0.01$ and in Fig. 3(b) for $\Delta x = 0.2$ and $\Delta \tilde{t} = 0.02$. It is evident that TSCN shows faster convergence than TSBE. As discussed in the Sec. 3.1.1, the TSBE does not lead to a unitary time evolution in contrast to TSCN. In order to confirm this, we consider the

Table 2: Comparison of ground state energies of pseudospin-1/2 BEC obtained with TSFS, TSBE and TSCN for $\Omega = 0.5$ and different values of γ . The results have been obtained with $\Delta x = 0.1$ and $\Delta \tilde{t} = 0.01$. The interaction strength parameters considered for q1D BEC are $g_{11} = 446.95$, $g_{22} = 402.26$ and $g_{12} = g_{21} = 491.65$, whereas the same for q2D BEC are $g_{11} = 250.52$, $g_{22} = 225.47$ and $g_{12} = g_{21} = 275.57$.

	γ	TSFS	TSBE	TSCN
q1D	0.5	21.4231	21.4231	21.4231
	1.0	21.4002	21.4002	21.4002
	1.5	21.3033	21.3034	21.3033
	2.0	20.6711	20.6727	20.6715
q2D	0.5	5.6457	5.6457	5.6457
	1.0	5.3339	5.3339	5.3339
	1.5	4.7181	4.7181	4.7181
	2.0	3.8434	3.8438	3.8438

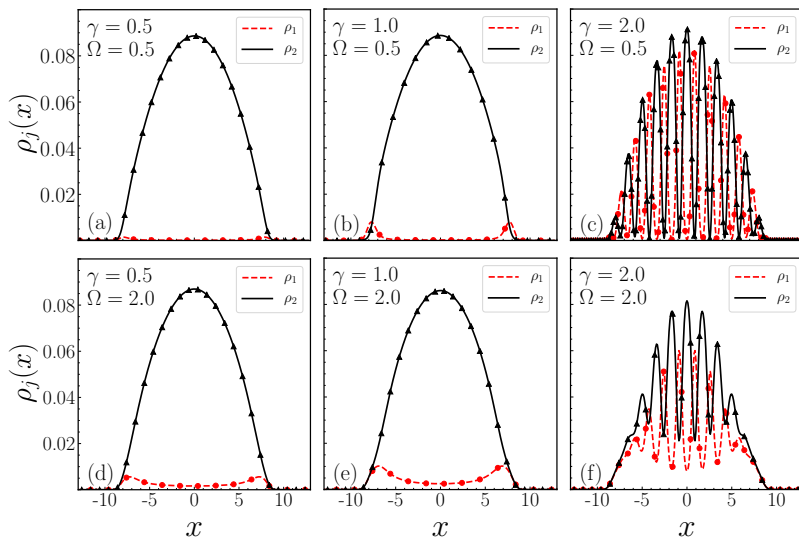


Figure 1: (Color online) (a)-(c) are the component densities for an SO-coupled q1D ^{87}Rb pseudospin- $\frac{1}{2}$ BEC with $\Omega = 0.5$ and $\gamma = 0.5, 1, 2$, respectively. The same for $\Omega = 2$ are shown in (d)-(f), respectively. The lines and points correspond to the results from TSBE and TSCN, respectively. The interaction strengths considered in (a)-(f) are $g_{22} = 0.9g_{11}$ and $g_{12} = 1.1g_{11}$ with $g_{11} = 446.95$.

real-time evolution of the ground state solution of the q1D ^{87}Rb shown in Fig. 1(a) with TSBE and TSCN. For this we consider the ground state solution corresponding to interaction parameters in Eq. (58) with $\gamma = \Omega = 0.5$ as the

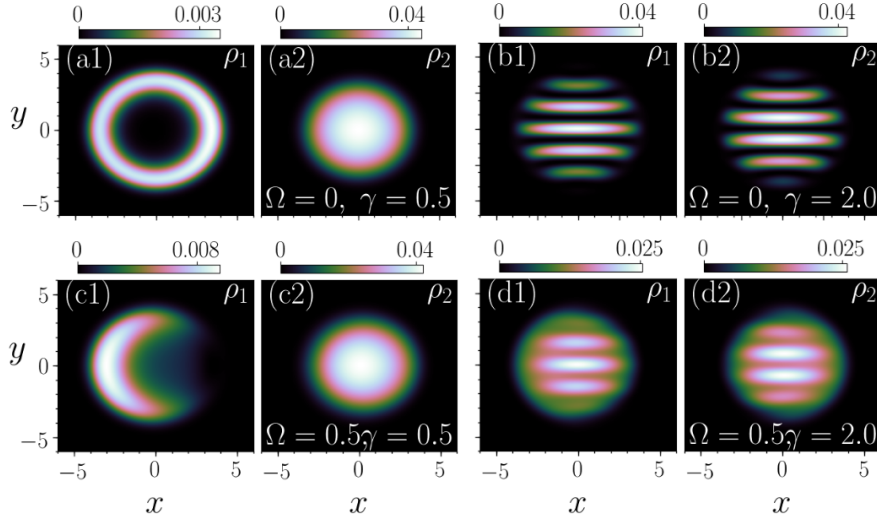


Figure 2: (Color online) (a1)-(a2) are the component densities obtained with TSCN method for an SO-coupled q2D ^{87}Rb pseudospin- $\frac{1}{2}$ BEC with $g_{11} = 250$, $g_{22} = 225$, $g_{12} = g_{21} = 275$, $\gamma = 0.5$ and $\Omega = 0$. The same for $(\gamma, \Omega) = (2, 0), (0.5, 0.5)$, and $(2, 0.5)$ are shown in (b1)-(b2), (c1)-(c2), and (d1)-(d2), respectively.

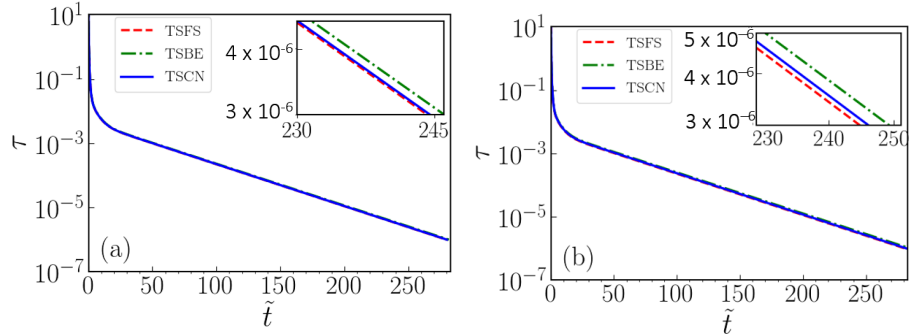


Figure 3: (Color online) The variation of convergence criterion during imaginary-time propagation to calculate the ground state of q1D ^{87}Rb . In (a), we have chosen $\Delta x = 0.1$ and $\Delta \tilde{t} = 0.01$, whereas for (b) $\Delta x = 0.2$ and $\Delta \tilde{t} = 0.02$.

initial solution at $t = 0$ in real-time evolution. The variation of total norm and energy as a function of time obtained using TSFS, TSBE, and TSCN are shown in Fig. 4(a)-(b), respectively. The non-conservation of norm and hence energy in TSBE makes the method unsuitable to study any realtime dynamics. The dynamics of the ground state, a stationary state, is trivial in the sense that besides norm and energy the expectation values of various operators are also conserved.

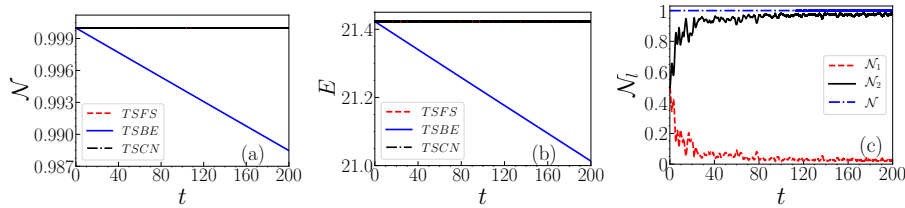


Figure 4: (Color online) (a) Norm \mathcal{N} as a function of time and (b) energy E as a function of time for the ground state solution of pseudospin-1/2 BEC of ^{87}Rb with $\gamma = \Omega = 0.5$. (c) Norm \mathcal{N} and \mathcal{N}_i as a function of time in realtime obtained for non-stationary initial solution using TSCN. The real-time evolution of initial solution is obtained using TSFS, TSBE and TSCN with $\Delta x = 0.1$ and $\Delta t = 0.005$.

Next, we consider the dynamics of non-stationary state using TSCN. We first obtain a non-stationary state by solving CGPEs for q1D ^{87}Rb with interaction strengths as defined in Eq. (58) and $\gamma = \Omega = 0.5$ under the constraint of zero polarization. The solution thus obtained is non-stationary, and is then evolved in realtime (without any additional constraint) using TSCN. The variation of component norms as a function of time is shown in Fig. 4(c).

4.2 Spin-1

We consider (1) ^{23}Na and (2) ^{87}Rb spin-1 BECs corresponding to antiferromagnetic and ferromagnetic phases in the absence of coupling. The scattering lengths corresponding to system (1) and (2) are $a_0 = 50.00a_B$, $a_1 = 55.01a_B$ [32] and $a_0 = 101.8a_B$, $a_1 = 100.4a_B$ [33], respectively. We consider 10000 atoms trapped in q1D trapping potential with $\omega_x = 2\pi \times 20\text{Hz}$, $\omega_y = \omega_z = 2\pi \times 400\text{Hz}$. The interaction strengths c_0 and c_2 in dimensionless units are given as

$$(1) \quad (c_0, c_2) = (240.83, 7.54), \quad (60a)$$

$$(2) \quad (c_0, c_2) = (885.72, -4.09). \quad (60b)$$

The same number of atoms trapped in q2D trapping potential with $\omega_x = \omega_y = 2\pi \times 20\text{Hz}$, $\omega_z = 2\pi \times 400\text{Hz}$ leads to following interaction strengths

$$(1) \quad (c_0, c_2) = (134.98, 4.22), \quad (61a)$$

$$(2) \quad (c_0, c_2) = (248.22, -1.15), \quad (61b)$$

for ^{23}Na and ^{87}Rb spin-1 BECs, respectively. The oscillator lengths for system (1) and (2) are $4.69 \mu\text{m}$ and $2.41 \mu\text{m}$, respectively. For these two cases, the comparison of ground state energies obtained from TSFS, TSBE and TSCN shows an excellent agreement as reported in Table-(3).

Table 3: Comparison of ground state energies of SO and coherently coupled spin-1 BECs using TSFS, TSBE, and TSCN methods with $\Delta x = 0.1$ and $\Delta t = 0.005$. The energies correspond to different values γ . The coherent coupling used for q1D and q2D systems are 0.5 and 0.1, respectively.

	γ	^{23}Na			^{87}Rb		
		TSFS	TSBE	TSCN	TSFS	TSBE	TSCN
q1D	0.5	15.0623	15.0623	15.0623	35.7812	35.7812	35.7812
	1.0	14.6873	14.6873	14.6873	35.4062	35.4062	35.4062
	1.5	14.0623	14.0623	14.0623	34.7812	34.7812	34.7812
	2.0	13.1873	13.1876	13.1876	34.9062	33.9062	33.9065
q2D	0.5	4.3797	4.3797	4.3797	8.2638	8.2638	8.2638
	1.0	3.9602	3.9602	3.9601	7.8747	7.8747	7.8747
	1.5	3.3303	3.3303	3.3303	7.2435	7.2435	7.2435
	2.0	2.4486	2.4489	2.4489	6.3658	6.3661	6.3661

The numerically obtained component densities in the ground states of harmonically trapped q1D ^{23}Na and ^{87}Rb spin-1 BECs with different values of γ and Ω are shown in Fig. 5. The component densities obtained using TSBE

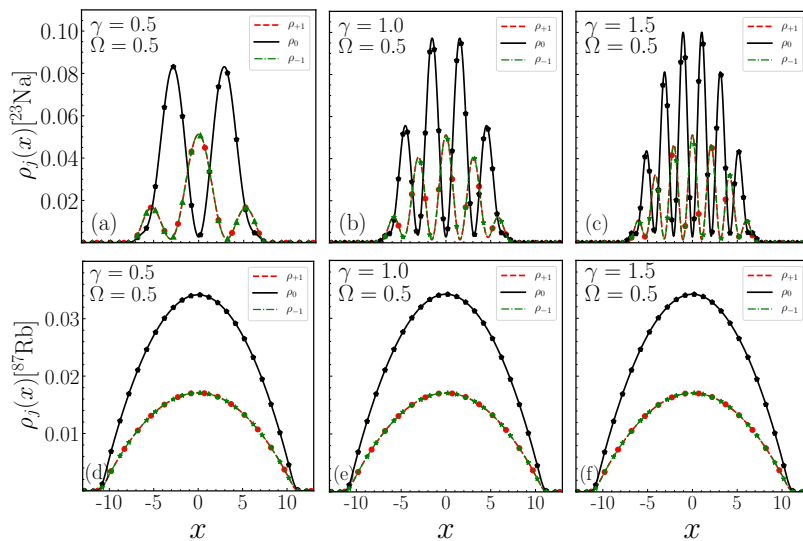


Figure 5: (Color online) (a)-(c) are the ground state component densities for an SO-coupled q1D ^{23}Na spin-1 BEC for different values γ and $\Omega = 0.5$. The same for ^{87}Rb spin-1 BEC are shown in (d)-(f). In (a)-(f), lines and points correspond to the results from TSBE and TSCN, respectively.

and TSCN are in an excellent agreement. Similarly, in Fig. (6) we have shown some distinct ground state density profiles for q2D ^{23}Na and ^{87}Rb spin-1 BECs obtained using TSCN.

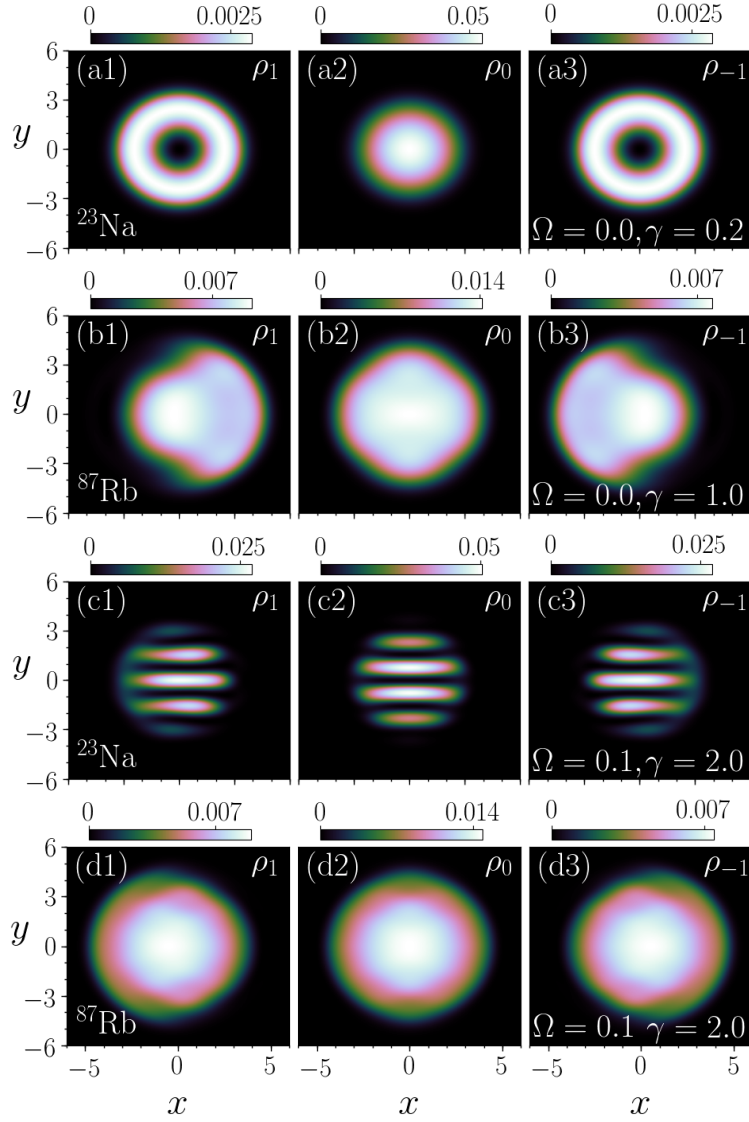


Figure 6: (Color online) (a1)-(a3) are the ground-state component densities for an SO-coupled q2D ^{23}Na spin-1 BEC with $\gamma = 0.2$ and $\Omega = 0$, whereas the same for ^{87}Rb are in (b1)-(b3). (c1)-(c3) and (d1)-(d3) are the ground-state component densities for ^{23}Na and ^{87}Rb BECs, respectively, with $\gamma = 2$ and $\Omega = 0.1$.

4.3 Spin-2

We consider (1) ^{83}Rb , (2) ^{23}Na , and (3) ^{87}Rb spin-2 BECs corresponding to ferromagnetic, anti-ferromagnetic and cyclic phases. The three sets of scattering

length corresponding to these systems are [18, 34]

$$(1) \quad a_0 = 83.0a_B, \quad a_2 = 82.0a_B, \quad a_4 = 81.0a_B; \quad (62)$$

$$(2) \quad a_0 = 34.9a_B, \quad a_2 = 45.8a_B, \quad a_4 = 64.5a_B; \quad (63)$$

$$(3) \quad a_0 = 87.93a_B, \quad a_2 = 91.28a_B, \quad a_4 = 99.18a_B, \quad (64)$$

respectively. We consider 10000 atoms of each of these systems trapped in q1D trapping potential with $\omega_x = 2\pi \times 20\text{Hz}$, $\omega_y = \omega_z = 2\pi \times 400\text{Hz}$. The interaction strengths c_0 , c_1 and c_2 in dimensionless units are given as

$$(1) \quad (c_0, c_1, c_2) = (699.62, -1.23, 4.90),$$

$$(2) \quad (c_0, c_1, c_2) = (242.97, 12.06, -13.03),$$

$$(3) \quad (c_0, c_1, c_2) = (831.26, 9.91, 0.31).$$

Similarly, we consider 10000 atoms of each of three systems trapped in a q2D trapping potential with $\omega_x = \omega_y = 2\pi \times 20\text{Hz}$, $\omega_z = 2\pi \times 400\text{Hz}$. The resultant interaction strengths for q2D ^{83}Rb , ^{23}Na , ^{87}Rb spin-2 BECs are

$$(1) \quad (c_0, c_1, c_2) = (392.14, -0.67, 2.74),$$

$$(2) \quad (c_0, c_1, c_2) = (136.18, 6.76, -7.30),$$

$$(3) \quad (c_0, c_1, c_2) = (465.92, 5.55, 0.18),$$

respectively. The oscillator lengths corresponding to three systems (1), (2) and (3) are $2.47 \mu\text{m}$, $4.69 \mu\text{m}$ and $2.41 \mu\text{m}$, respectively. For these set of parameters, the ground state energies obtained with TSFS, TSBE, and TSCN are reported in Table 4. The agreement between the results with three methods is very good.

Table 4: Comparison of ground state energies of q1D and q2D spin-2 BECs of ^{83}Rb , ^{23}Na and ^{87}Rb obtained with TSFS, TSBE, and TSCN using $\Delta x = 0.1$ and $\Delta \tilde{t} = 0.001$ for different values of γ and Ω .

	(γ, Ω)	^{83}Rb			^{23}Na			^{87}Rb		
		TSFS	TSBE	TSCN	TSFS	TSBE	TSCN	TSFS	TSBE	TSCN
q1D	(0.5,0.5)	29.8496	29.8496	29.8496	14.6877	14.6877	14.6877	34.2036	34.2036	34.2036
	(1.0,0.5)	28.3496	28.3499	28.3499	13.1877	13.1881	13.1881	32.7036	32.7039	32.7039
q2D	(0.5,0.1)	7.0875	7.0875	7.0875	3.9648	3.9645	3.9645	7.6850	7.6850	7.6850

Similarly, the ground-state component densities of q1D spin-2 ^{83}Rb , ^{23}Na , and ^{87}Rb BECs with different values of γ and Ω calculated using TSBE and TSCN are in very good agreement as shown in Fig. (7). In q2D spin-2 BECs also, ground-state component densities calculated using three methods are in a very good agreement. Here we illustrate some qualitatively distinct ground-state density profiles obtained with TSCN. The component densities in the ground state of q2D ^{83}Rb , ^{23}Na , and ^{87}Rb spin-2 BECs with $\gamma = 0.5$ and $\Omega = 0.1$ are shown in Fig. 8. The ground state of ^{83}Rb and ^{23}Na spin-2 BECs have vortices of winding number $-1, 0, +1, +2, +3$ and $-2, -1, 0, +1, +2$ associated

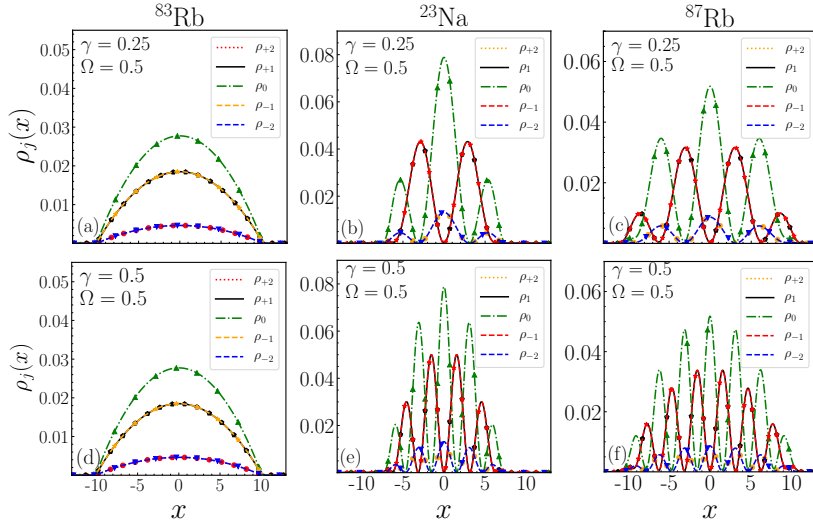


Figure 7: (Color online) (a)-(c) are the ground-state component densities for SO-coupled quasi-1D ^{83}Rb , ^{23}Na and ^{87}Rb spin-2 BEC with $\gamma = 0.25$ and $\Omega = 0.5$ respectively, whereas (d)-(f) are the same for $\gamma = 0.5$ and $\Omega = 0.5$. In (a)-(f), lines and points correspond to densities with TSBE and TSCN, respectively.

with the $l = 2, 1, 0, -1, -2$ components, respectively. The ground state of q2D ^{87}Rb spin-2 BEC has stripe pattern in component densities for $\gamma = 0.5$ and $\Omega = 0.1$.

For q2D ^{87}Rb spin-2 BEC, the ground state component densities with $\gamma = 1, \Omega = 0$ and $\gamma = 2, \Omega = 0$ are also illustrated in Figs. 9(a1)-(a5) and Figs. 9(b1)-(b5), respectively. The ground-state component densities have triangular lattice pattern for $\gamma = 1$ and stripe density pattern for $\gamma = 2$.

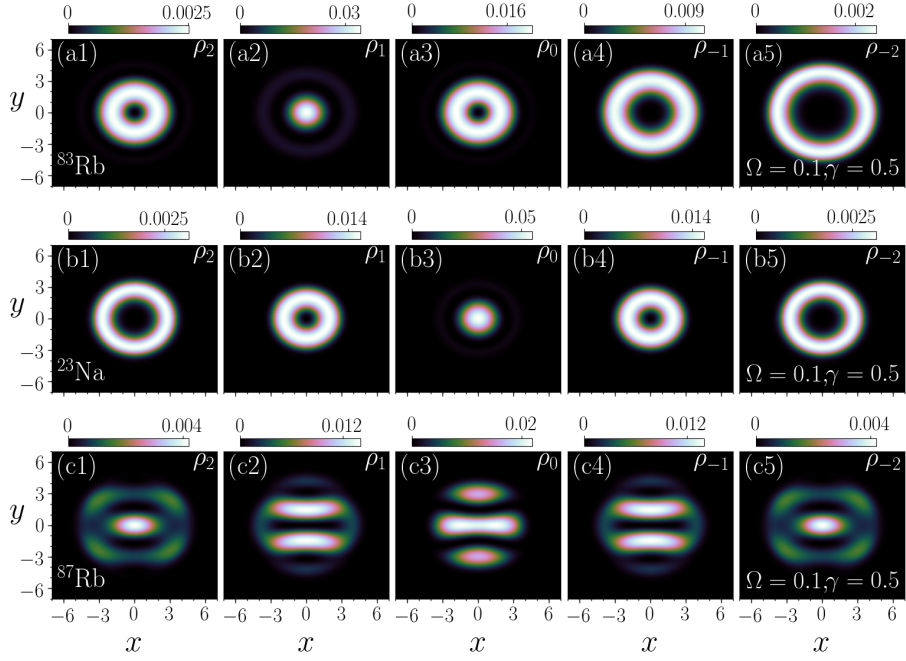


Figure 8: (Color online) (a1)-(a5) are the component densities for an SO-coupled quasi-2D ^{83}Rb , (b1)-(b5) are for ^{23}Na and (c1)-(c5) are for ^{87}Rb spin-2 BEC with $\Omega = 0.1$, and $\gamma = 0.5$ respectively.

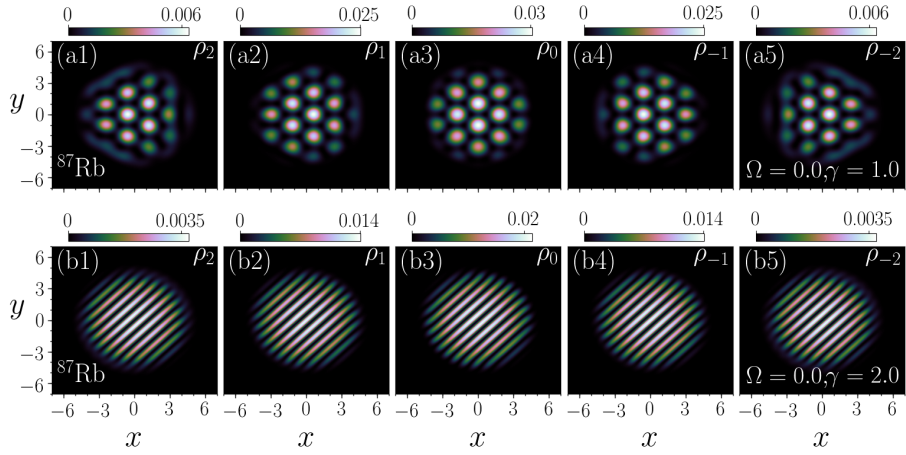


Figure 9: (Color online) (a1)-(a5) are the component densities for an SO-coupled quasi-2D ^{87}Rb with $\gamma = 1.0$ whereas (b1)-(b5) are for same system with $\gamma = 2.0$ respectively.

Summary

We have discussed time-splitting Backward-Euler and Crank-Nicolson methods to study the SO-coupled spinor BECs with coherent coupling. We have developed the methods for pseudospin-1/2, spin-1 and spin-2 BEC in q1D and q2D traps. We have considered Rashba SO coupling in the present work, one can also consider Dresselhaus coupling or a combination of both within the framework of same numerical schemes. We have compared the results obtained with these finite difference methods with the time-splitting Fourier spectral method. The numerical results for stationary states obtained with the three methods are in very good agreement. We have provided the comparison of ground state energies and component density profiles calculated using three methods for several illustrative cases. In imaginary-time propagation, TSCN shows faster convergence as compared to TSBE. Moreover, the time evolution as per TSCN is unitary time evolution consistent with the underlying Hermitian Hamiltonian. This is not the case with TSBE which results in non-unitary time evolution and thus rendering the method not suitable to the study any real-time dynamics. The finite difference methods developed in the present work can be easily extended to higher spin system like spin-3 BEC.

Appendix

The split equation for $H_{\text{nd}+}$ is

$$i\frac{\partial\Psi}{\partial t} = H_{\text{nd}+}\Psi \quad (65)$$

where

$$H_{\text{nd}+} = \begin{pmatrix} 0 & h_{12} & h_{13} & 0 & 0 \\ h_{12}^* & 0 & h_{23} & 0 & 0 \\ h_{13}^* & h_{23}^* & 0 & h_{34} & h_{35} \\ 0 & 0 & h_{34}^* & 0 & h_{45} \\ 0 & 0 & h_{35}^* & h_{45}^* & 0 \end{pmatrix}, \quad (66)$$

Eq. (66) can split into two operator H_1 and H_2

$$H_1 = \begin{pmatrix} 0 & h_{12} & 0 & 0 & 0 \\ h_{12}^* & 0 & h_{23} & 0 & 0 \\ 0 & h_{23}^* & 0 & h_{34} & 0 \\ 0 & 0 & h_{34}^* & 0 & h_{45} \\ 0 & 0 & 0 & h_{45}^* & 0 \end{pmatrix}, \quad H_2 = \begin{pmatrix} 0 & 0 & h_{13} & 0 & 0 \\ 0 & 0 & 0 & 0 & 0 \\ h_{13}^* & 0 & 0 & 0 & h_{35} \\ 0 & 0 & 0 & 0 & 0 \\ 0 & 0 & h_{35}^* & 0 & 0 \end{pmatrix}, \quad (67)$$

where

$$\begin{aligned} h_{12} &= c_1 F_- - \frac{2}{5} c_2 \psi_{-1} \psi_{-2}^* + \frac{\Omega}{2}, & h_{23} &= \frac{\sqrt{6}}{2} c_1 F_- - \frac{1}{5} c_2 \psi_0 \psi_{-1}^* + \frac{\sqrt{6}\Omega}{4}, \\ h_{34} &= \frac{\sqrt{6}}{2} c_1 F_- - \frac{1}{5} c_2 \psi_1 \psi_0^* + \frac{\sqrt{6}\Omega}{4}, & h_{45} &= c_1 F_- - \frac{2}{5} c_2 \psi_2 \psi_1^* + \frac{\Omega}{2}, \\ h_{13} &= \frac{1}{5} c_2 \psi_0 \psi_{-2}^*, & h_{35} &= \frac{1}{5} c_2 \psi_2 \psi_0^*. \end{aligned}$$

The approximate solution of Eq. (65) is given by

$$\begin{aligned}
\Psi(x, t + \delta t) &= \exp(-iH_{\text{nd}+}dt) \Psi(x, t), \\
&\approx \exp(-iH_2dt) \exp(-iH_1dt) \Psi(x, t), \\
&= \exp(-i\delta t P A_2 P^{-1}) \exp(-i\delta t S A_1 S^{-1}) \Psi(x, t), \\
&= P \exp(-i\delta t A_2) P^{-1} S \exp(-i\delta t A_1) S^{-1} \Psi(x, t), \quad (68)
\end{aligned}$$

where 5×5 matrix

$$S = (u_1, u_2, u_3, u_4, u_5).$$

The $(u_1, u_2, u_3, u_4, u_5)$ are normalised eigen vectors which can be obtained from un-normalised eigen vectors $(v_1, v_2, v_3, v_4, v_5)$, defined as

$$\begin{aligned}
v_1 &= \left[\frac{h_{23}h_{45}}{h_{12}^*h_{34}^*}, 0, -\frac{h_{45}}{h_{34}^*}, 0, 1 \right]^T, \\
v_2 &= \left[\frac{h_{12}(-\alpha^2 + \beta^2 + 2|h_{12}|^2 + 2|h_{23}|^2 - 2|h_{34}|^2 - 2|h_{45}|^2)}{4h_{23}^*h_{34}^*h_{45}^*}, \right. \\
&\quad \frac{\beta(\alpha^2 - \beta^2 + 2|h_{12}|^2 - 2|h_{23}|^2 + 2|h_{34}|^2 + 2|h_{45}|^2)}{4\sqrt{2}h_{23}^*h_{34}^*h_{45}^*}, \\
&\quad \left. \frac{(-\alpha^2 + \beta^2 + 2|h_{12}|^2 + 2|h_{23}|^2 + 2|h_{34}|^2 - 2|h_{45}|^2)}{4h_{34}^*h_{45}^*}, -\frac{\beta}{\sqrt{2}h_{45}^*}, 1 \right]^T, \\
v_3 &= \left[\frac{h_{12}(-\alpha^2 + \beta^2 + 2|h_{12}|^2 + 2|h_{23}|^2 - 2|h_{34}|^2 - 2|h_{45}|^2)}{4h_{23}^*h_{34}^*h_{45}^*}, \right. \\
&\quad -\frac{\beta(\alpha^2 - \beta^2 + 2|h_{12}|^2 - 2|h_{23}|^2 + 2|h_{34}|^2 + 2|h_{45}|^2)}{4\sqrt{2}h_{23}^*h_{34}^*h_{45}^*}, \\
&\quad \left. \frac{(-\alpha^2 + \beta^2 + 2|h_{12}|^2 + 2|h_{23}|^2 + 2|h_{34}|^2 - 2|h_{45}|^2)}{4h_{34}^*h_{45}^*}, \frac{\beta}{\sqrt{2}h_{45}^*}, 1 \right]^T, \\
v_4 &= \left[\frac{h_{12}(\alpha^2 - \beta^2 + 2|h_{12}|^2 + 2|h_{23}|^2 - 2|h_{34}|^2 - 2|h_{45}|^2)}{4h_{23}^*h_{34}^*h_{45}^*}, \right. \\
&\quad \frac{\alpha(-\alpha^2 + \beta^2 + 2|h_{12}|^2 - 2|h_{23}|^2 + 2|h_{34}|^2 + 2|h_{45}|^2)}{4\sqrt{2}h_{23}^*h_{34}^*h_{45}^*}, \\
&\quad \left. \frac{(\alpha^2 - \beta^2 + 2|h_{12}|^2 + 2|h_{23}|^2 + 2|h_{34}|^2 - 2|h_{45}|^2)}{4h_{34}^*h_{45}^*}, -\frac{\alpha}{\sqrt{2}h_{45}^*}, 1 \right]^T, \\
v_5 &= \left[\frac{h_{12}(\alpha^2 - \beta^2 + 2|h_{12}|^2 + 2|h_{23}|^2 - 2|h_{34}|^2 - 2|h_{45}|^2)}{4h_{23}^*h_{34}^*h_{45}^*}, \right. \\
&\quad -\frac{\alpha(-\alpha^2 + \beta^2 + 2|h_{12}|^2 - 2|h_{23}|^2 + 2|h_{34}|^2 + 2|h_{45}|^2)}{4\sqrt{2}h_{23}^*h_{34}^*h_{45}^*}, \\
&\quad \left. \frac{(\alpha^2 - \beta^2 + 2|h_{12}|^2 + 2|h_{23}|^2 + 2|h_{34}|^2 - 2|h_{45}|^2)}{4h_{34}^*h_{45}^*}, \frac{\alpha}{\sqrt{2}h_{45}^*}, 1 \right]^T, \quad (69)
\end{aligned}$$

by using Gram-Schmidt orthogonalization. The matrix

$$A_1 = \text{diag} \left(0, -\frac{\beta}{\sqrt{2}}, \frac{\beta}{\sqrt{2}}, -\frac{\alpha}{\sqrt{2}}, \frac{\alpha}{\sqrt{2}} \right), \quad (70)$$

where

$$\begin{aligned} \alpha^2 &= \sqrt{(|h_{12}|^2 + |h_{23}|^2 + |h_{34}|^2 + |h_{45}|^2)^2 - 4(|h_{12}|^2|h_{34}|^2 + |h_{45}|^2(|h_{12}|^2 + |h_{23}|^2))} \\ &\quad + |h_{12}|^2 + |h_{23}|^2 + |h_{34}|^2 + |h_{45}|^2, \\ \beta^2 &= -\sqrt{(|h_{12}|^2 + |h_{23}|^2 + |h_{34}|^2 + |h_{45}|^2)^2 - 4(|h_{12}|^2|h_{34}|^2 + |h_{45}|^2(|h_{12}|^2 + |h_{23}|^2))} \\ &\quad + |h_{12}|^2 + |h_{23}|^2 + |h_{34}|^2 + |h_{45}|^2. \end{aligned}$$

Similarly, 5×5 matrix

$$P = (w_1, w_2, w_3, w_4, w_5),$$

where

$$\begin{aligned} w_1 &= \left[-\frac{h_{35}|h_{13}|}{h_{13}^* \sqrt{|h_{13}|^2 + |h_{35}|^2}}, 0, 0, 0, \frac{1}{\sqrt{\frac{h_{35}h_{35}^*}{|h_{13}|^2} + 1}} \right]^T, \\ w_2 &= [0, 0, 0, 1, 0]^T, \quad w_3 = [0, 1, 0, 0, 0]^T, \\ w_4 &= \left[\frac{h_{13}|h_{35}|}{\sqrt{2}h_{35}^* \sqrt{|h_{13}|^2 + |h_{35}|^2}}, 0, -\frac{|h_{35}|}{\sqrt{2}h_{35}^*}, 0, \frac{|h_{35}|}{\sqrt{2}\sqrt{|h_{13}|^2 + |h_{35}|^2}} \right]^T, \\ w_5 &= \left[\frac{h_{13}|h_{35}|}{\sqrt{2}h_{35}^* \sqrt{|h_{13}|^2 + |h_{35}|^2}}, 0, \frac{|h_{35}|}{\sqrt{2}h_{35}^*}, 0, \frac{|h_{35}|}{\sqrt{2}\sqrt{|h_{13}|^2 + |h_{35}|^2}} \right]^T, \quad (71) \end{aligned}$$

and 5×5 matrix

$$A_2 = \text{diag} \left(0, 0, 0, -\sqrt{|h_{13}|^2 + |h_{35}|^2}, \sqrt{|h_{13}|^2 + |h_{35}|^2} \right). \quad (72)$$

References

- [1] D.M. Stamper-Kurn, M.R. Andrews, A.P. Chikkatur, S. Inouye, H.-J. Miesner, J. Stenger, W. Ketterle, Phys. Rev. Lett. **80** (1998) 2027.
- [2] J. Stenger, S. Inouye, D.M. Stamper-Kurn, H.J. Miesner, A.P. Chikkatur, W. Ketterle, Nature, **396** (1998) 345.
- [3] Y. Kawaguchi, M. Ueda, Physics Reports **520** (2012) 253.
- [4] D.M. Stamper-Kurn, M. Ueda, Rev. Mod. Phys. **85** (2013) 1191.
- [5] C.J. Myatt, E.A. Burt, R.W. Ghrist, E.A. Cornell, C.E. Wieman, Phys. Rev. Lett. **78** (1997) 586.
- [6] M.S. Chang, C.D. Hamley, M.D. Barrett, J.A. Sauer, K.M. Fortier, W. Zhang, L. You, and M.S. Chapman, Phys. Rev. Lett. **92** (2004) 140403.

- [7] A. Görlitz, T.L. Gustavson, A.E. Leanhardt, R. Löw, A.P. Chikkatur, S. Gupta, S. Inouye, D.E. Pritchard and W. Ketterle Phys. Rev. Lett. **90** (2003) 090401.
- [8] B. Pasquiou, E. Maréchal, G. Bismut, P. Pedri, L. Vernac, O. Gorceix, B. Laburthe-Tolra, Phys. Rev. Lett. **106** (2011) 255303.
- [9] Y.-J. Lin, K. Jiménez-García, I.B. Spielman, Nature **471** (2011) 83.
- [10] K. Osterloh, M. Baig, L. Santos, P. Zoller, M. Lewenstein, Phys. Rev. Lett. **95** (2005) 010403.
- [11] J. Ruseckas, G. Juzeliunas, P. Öhberg, M. Fleischhauer, Phys. Rev. Lett. **95** (2005) 010404.
- [12] N. Goldman, G. Juzeliunas, P. Öhberg, I.B. Spielman, Rep. Prog. Phys. **77** (2014) 126401.
- [13] V. Galitski, I.B. Spielman, Nature, **494** (2013) 49.
- [14] C. Wang, C. Gao, C.-M. Jian, H. Zhai, Phys. Rev. Lett. **105** (2010) 160403.
- [15] Y. Li, L.P. Pitaevskii, S. Stringari, Phys. Rev. Lett. **108** 225301 (2012).
- [16] H. Zhai, Physics Reports **78** (2015) 026001.
- [17] T. L. Ho, Phys. Rev. Lett. **81** (1998) 742.
- [18] C.V. Ciobanu, S. Yip, T. Ho, Phys. Rev. A **61** (2000) 033607.
- [19] S.-M. Chang, W.-W. Lin, and S.-F. Shieh, J. Comp. Phys. **202** (2005) 367.
- [20] W. Bao and J. Shen, SIAM Journal on Scientific Computing **26** (2005) 2010.
- [21] W. Bao, Multiscale Model. Simul., **2** (2004) 210236.
- [22] S. Ashhab and C. Lobo, Phys. Rev. A, **66** (2002) 013609.
- [23] H. Wang, Int. J. Comp. Math. **84** (2007) 925.
- [24] W. Bao and F.Y. Lim, F. Y., SIAM Journal on Scientific Computing **30** (2008) 1925.
- [25] W. Bao, I.-L. Chern, and Y. Zhang, J. Comp. Phys. **253** (2013) 189.
- [26] H. Wang and Z. Xu, Comp. Phys. Comm. **185** (2014) 2803; H. Wang, J. Comp. Phys. **274** (2014) 473.
- [27] P. Kaur, A. Roy, and S. Gautam, Comp. Phys. Comm. **259** (2021) 107671.
- [28] P. Banger, P. Kaur, A. Roy, and S. Gautam, arXiv preprint arXiv:2011.08892 (2020).
- [29] T. Ohmi, K. Machida, J. Phys. Soc. Japan **67** (1998) 1822.
- [30] R. L. Burden and J. D. Faires, “Numerical Analysis,” 9th Edition, Brooks/Cole, Pacific Grove, 2011.

- [31] M. Rezghi, E. Elden, *Linear Algebra and its Application*, **435** (2011) 422447.
- [32] A. Crubellier, O. Dulieu, F. Masnou-Seeuws, M. Elbs, H. Knöckel, E. Tiemann, *Eur. Phys. J. D* **6** (1999) 211.
- [33] E.G.M. van Kempen, S.J.J.M.F. Kokkelmans, D.J. Heinzen, B.J. Verhaar, *Phys. Rev. Lett.* **88** (2002) 093201.
- [34] A. Widera, F. Gerbier, S. Fölling, T. Gericke, O. Tatjana and I. Bloch, *New Journal of Physics* **8** (2006) 152.